

Award Number: W81XWH-16-1-0538

TITLE: Direct Regulation of Estrogen Receptor Transcriptional Activity by NF1

PRINCIPAL INVESTIGATOR: Eric Chang

CONTRACTING ORGANIZATION: Baylor College of Medicine
Houston, TX 77030

REPORT DATE: October 2019

TYPE OF REPORT: Annual

PREPARED FOR: U.S. Army Medical Research and Materiel Command
Fort Detrick, Maryland 21702-5012

DISTRIBUTION STATEMENT: Approved for Public Release;
Distribution Unlimited

The views, opinions and/or findings contained in this report are those of the author(s) and should not be construed as an official Department of the Army position, policy or decision unless so designated by other documentation.

REPORT DOCUMENTATION PAGE

Form Approved
OMB No. 0704-0188

Public reporting burden for this collection of information is estimated to average 1 hour per response, including the time for reviewing instructions, searching existing data sources, gathering and maintaining the data needed, and completing and reviewing this collection of information. Send comments regarding this burden estimate or any other aspect of this collection of information, including suggestions for reducing this burden to Department of Defense, Washington Headquarters Services, Directorate for Information Operations and Reports (0704-0188), 1215 Jefferson Davis Highway, Suite 1204, Arlington, VA 22202-4302. Respondents should be aware that notwithstanding any other provision of law, no person shall be subject to any penalty for failing to comply with a collection of information if it does not display a currently valid OMB control number. **PLEASE DO NOT RETURN YOUR FORM TO THE ABOVE ADDRESS.**

1. REPORT DATE Oct 2019		2. REPORT TYPE Annual		3. DATES COVERED 09/30/2018 - 09/29/2019	
4. TITLE AND SUBTITLE Direct Regulation of Estrogen Receptor Transcriptional Activity by NF1				5a. CONTRACT NUMBER	
				5b. GRANT NUMBER W81XWH-16-1-0539	
				5c. PROGRAM ELEMENT NUMBER	
6. AUTHOR(S) Eric Chang and Matthew Ellis E-Mail: echang1@bcm.edu ; matthew.ellis@bcm.edu				5d. PROJECT NUMBER	
				5e. TASK NUMBER	
				5f. WORK UNIT NUMBER	
7. PERFORMING ORGANIZATION NAME(S) AND ADDRESS(ES) Baylor College of Medicine One Baylor Plaza, BCM600 Houston, TX 77030-3411				8. PERFORMING ORGANIZATION REPORT NUMBER	
9. SPONSORING / MONITORING AGENCY NAME(S) AND ADDRESS(ES) U.S. Army Medical Research and Materiel Command Fort Detrick, Maryland 21702-5012				10. SPONSOR/MONITOR'S ACRONYM(S)	
				11. SPONSOR/MONITOR'S REPORT NUMBER(S)	
12. DISTRIBUTION / AVAILABILITY STATEMENT Approved for Public Release; Distribution Unlimited					
13. SUPPLEMENTARY NOTES					
14. ABSTRACT The key objective of this project is to define a resistance mechanism for treating ER+ breast cancer by endocrine therapy, such as tamoxifen. This project was guided by a clinical study searching for driver mutations that promote resistance to tamoxifen, leading to the discovery that inactivating NF1 (neurofibromin) is a key factor driving resistance. This project investigates the hypothesis that inactivating NF1, previously best known as a negative regulator for Ras by acting as a GAP (GTPase Activating Protein), can not only activate Ras, but also ER by interacting with ER's co-regulators. This is a collaboration between two PIs with complementary expertise. Dr. Chang is a molecular biologist and responsible for Aim 1, which is to investigate NF1's interaction with known ER co-regulator. Dr. Ellis is a physician scientist who is responsible for Aim 2 to establish a treatment strategy to treat NF1-deficient ER+ breast cancer. We have made great stride in this project period from both aims. Briefly, we have uncovered a surprising GAP-independent activity of NF1 that it is also a co-repressor for ER. This is backed by technologically sophisticated RNA-seq and ChIP-seq experiments. As such, inactivating a single tumor suppressor NF1 can activate two powerful oncogenic pathways, which must be co-targeted for effective treatment. To this end, we demonstrate that using patient-derived xenograft model that this can be achieved by FDA-approved fulvestrant in combination with dabrafenib and trametinib.					
15. SUBJECT TERMS NF1, Neurofibromatosis type 1, Ras GTPase, GAP, Neurofibromin, estrogen receptor, gene expression, targeted therapy, ER co-regulators, ER-co-repressors.					
16. SECURITY CLASSIFICATION OF:			17. LIMITATION OF ABSTRACT	18. NUMBER OF PAGES	19a. NAME OF RESPONSIBLE PERSON
a. REPORT	b. ABSTRACT	c. THIS PAGE			19b. TELEPHONE NUMBER (include area code)
Classified	Unclassified	Unclassified	Unclassified		USAMRMC

Table of Contents

	<u>Page</u>
1. Introduction.....	2
2. Keywords.....	2
3. Accomplishments.....	2
4. Impact.....	5
5. Changes/Problems.....	5
6. Products.....	5
7. Participants & Other Collaborating Organizations.....	6
8. Special Reporting Requirements.....	6
9. Appendices.....	6

INTRODUCTION

Our overarching **objectives** are to define mechanisms of endocrine therapy resistance, and to design etiology-matched treatments to improve outcomes in estrogen receptor α positive (ER⁺) breast cancer. It is **hypothesized** that the *NF1* (Neurofibromatosis type 1) gene, which encodes neurofibromin, best known chiefly as a negative regulator for Ras as a GAP (GTPase Activating Protein), also negatively regulates ER signaling via co-activator interactions. As a result, NF1 loss in tumors is expected to induce aggressive tumor behavior not only through activated Ras signaling but also through increased ER activity. This project is funded as a multi-PI grant with Eric Chang as the initiating PI, who is responsible for the molecular study as proposed in Aim 1, and Matthew Ellis as the Patterning PI who is responsible for preclinical therapeutic study using animals as proposed in Aim 2. We have made great strides and a manuscript describing our findings has been conditionally accepted by *Cancer Cell*, and we have received new funding supported by preliminary data generated by this project (see “Products”). Our task-specific progress is as follows:

KEYWORDS

NF1, Neurofibromatosis type 1, Ras GTPase, GAP, Neurofibromin, estrogen receptor, gene expression, targeted therapy. ER co-regulators, ER-co-repressors.

ACCOMPLISHMENTS

This proposal has two specific aims: In **Aim 1** we will define how NF1 regulates expression of ER target genes by investigating a direct interaction between NF1 and canonical ER transcriptional co-regulators. This is the main responsibility of the Chang lab. **Aim 2** is the main responsibility of the Ellis lab centering on establishing a strategy to effectively treat NF1-deficient ER⁺ breast cancers by rationally combining anti-Ras and anti-ER approaches. As such, animal modeling is a chief focus of Aim 2.

Major Task 1 (responsibility of the Chang lab): To define how NF1 regulates expression of ER target genes by investigating a direct interaction between NF1 and canonical ER transcriptional co-regulators.

The key findings in Task 1 have led to a model that NF1 is not only a Ras GAP, but also a direct ER co-repressor for gene expression control. This is the main conclusion in a paper (Zheng et al, attached) that has been conditionally accepted for publication by the high impact journal *Cancer Cell*. Below we will outline the key data in that paper:

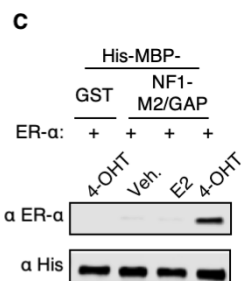


Figure 1. Direct binding between NF1 and ER.

1. NF1 binds ER directly in a ligand-dependent manner (Sub-task 4 and 10). We found that NF1 has two Leu/Ile rich co-repressor motifs called M1 and M2. When NF1's M2 domain was purified from bacteria, it binds purified ER in a tamoxifen (4-OHT)-dependent manner (Figure 1, which was presented in the paper as Figure 3C), agreeing with co-receptor properties. Such binding has also been validated in the paper by co-immunoprecipitation in breast cancer cell lines.

2. NF1 depletion enhances ER transcriptional activity as measured by RNA-seq (Sub-task 1 and 7). Agreeing with NF1 being an authentic

ER co-repressor, when *NF1* is silenced by DOX-inducible shRNA or knocked out by the CRISPR approach, the resulting cells show greatly enhanced expression of known estradiol (E2)-regulated genes as measured by RNA-seq, which was already reported in previous progress report (and shown as Figure 2A in Zheng et al).

We investigated whether NF1 represses ER recruitment to the ERE as a mechanism by which NF1-loss enhances expression of E2-responsive genes. We thus performed ER ChIP after NF1 depletion, and ER recruitment with or without estradiol (E2) stimulation to 10 ERE sites

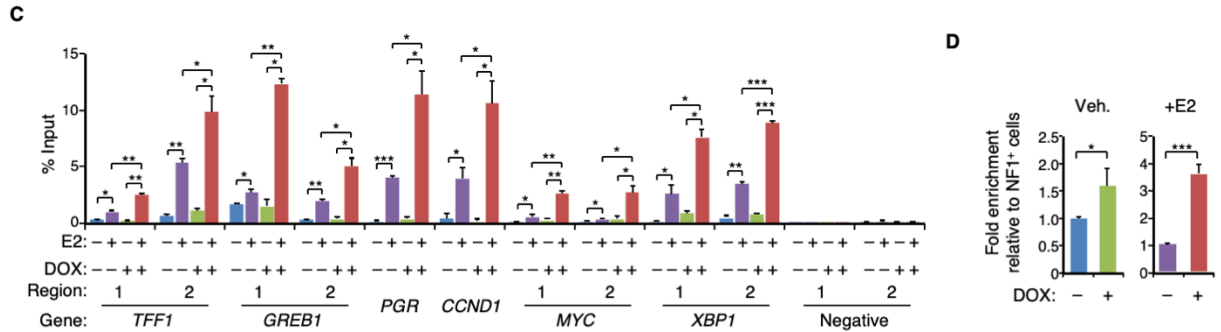


Figure 2. Enhanced ER recruitment to the ERE by *NF1* depletion.

was measured by qPCR. As shown in Figure 1 (and Figure 2C in the paper), NF1 deletion greatly enhanced ER recruitment to the EREs. This effect can even be seen when the cells were seeded in estrogen-deprived medium.

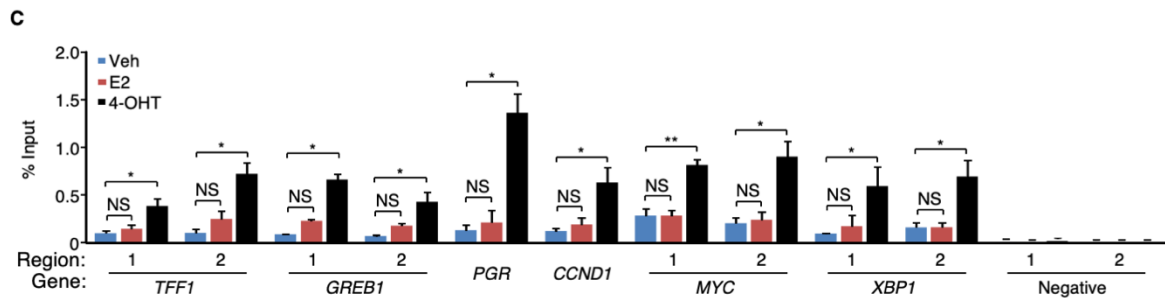


Figure 3. Tamoxifen-induced NF1 recruitment to EREs.

3. NF1 is recruited to the ERE driven by tamoxifen (Sub-task 5/6). We performed NF1 ChIP experiments and analyzed NF1 recruitment to 10 ERE sites (see Figure 2 above) by qPCR. This data is shown in Figure 5 in the paper, and one panel is presented here as Figure 3. As expected for a co-repressor, NF1 recruitment to the EREs is more strongly induced by the E2 antagonist tamoxifen.

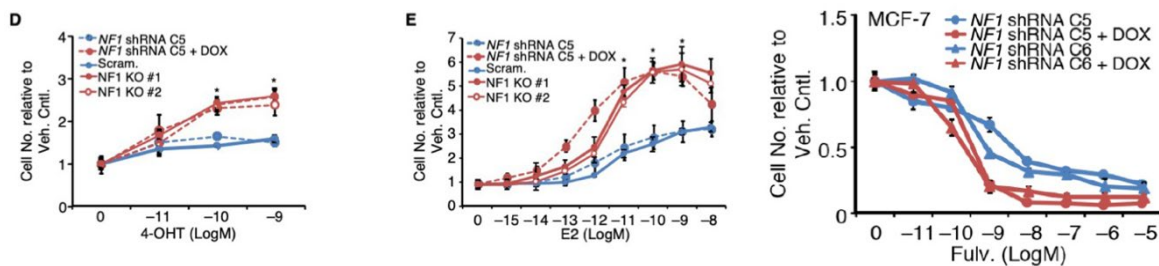


Figure 4. NF1-depletion induces resistance to both AI and tamoxifen, but retains sensitivity to a SERD, fulvestrant.

4. NF1-depleted cells show E2 hypersensitivity and tamoxifen agonism (Sub-task 7). Apparently due to enhance ER/E2-dependent gene expression, NF1-depletion permits ER⁺ breast cancer cells to grow in the presence of lower levels of E2 and turns tamoxifen into an agonist. An example of such response *in vitro* is shown in Figure 4 (which is part of Figure 1 in the paper). These laboratory observations explain why NF1-deficient ER⁺ breast patients are resistant to aromatase inhibitor (AI) and tamoxifen (See Figure 1 B and C in the paper). Importantly, these NF1-depleted cells still respond to fulvestrant, a SERD (Selective ER degrader, Figure 3), which offers a window of opportunity to initially treat NF1-deficient tumors. More of this will be discussed in Task-2.

5. ER interaction is independent of the GAP activity in NF1 (Sub-task-2). We used site-directed

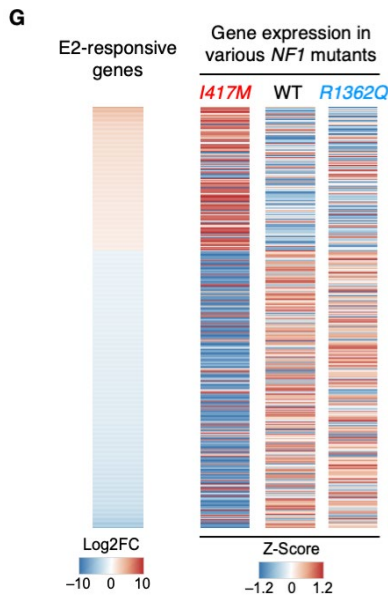


Figure 5. Enhanced expression of E2-responsive genes is selectively detected in NF1 mutant cells that are defective in ER-binding.

mutagenesis to selectively inactivate ER binding (by mutating M1 or M2) or the GAP activity, and found that the former enhances ER transcriptional activity without affecting GAP activity while the latter enhances Ras signaling activity without impacting ER binding. These findings are described in detail in Figure 3 of the paper. In this report, we show gene expression results from analyzing knock-in mutant MCF-7 cells in which both copies of the *NF1* genes were mutated by CRISPR. One example of this experiment is shown in Figure 5 (Figure 3G in the paper) in which RNA-seq was performed on MCF-7 cells carrying *NF1* mutant defective in ER binding (NF1-I417M) or GAP activity (NF1-R1362Q), as well as wild type MCF-7 cells, and the data show that expression of E2-responsive genes are greatly increase in the former. In contrast, the GAP mutant cells behave like wild type cells.

Major Task 2 (Responsibility of the Ellis lab): To establish a strategy to treat NF1-deficient ER⁺ breast cancers by rationally combining anti-Ras and anti-ER approaches.

1. ER⁺ NF1-deficient breast cancer can be effectively treated by a SERD combined with a MEK inhibitor (Sub-tasks 3, 5-9).

While ER⁺ NF1⁻ tumors should not be treated by AI or tamoxifen,

degrading ER itself by a SERD, fulvestrant, is an effective treatment (see Figure 4 above) at least initially. However, efficient Ras activation brought upon by NF1 loss later turns on cell survival pathways to bypass the ER blockade. We found an ER⁺ NF1⁻ PDX model (WHIM16) which is fulvestrant (F)-resistant (Figure 6, an earlier version of this experiment is presented in the paper as Figure 6C). The key Ras pathway responsive for this survival activity is apparently the Raf-MEK-ERK pathway, which can be blocked by a MEK inhibitor (MEKi). In fact, when a MEKi, selumetinib (S) or binimetinib (B), is combined with fulvestrant (F), full tumor regression can be detected in this ER⁺ NF1⁻ PDX model. A black arrow marks the time at which binimetinib was added to tumors treated with fulvestrant monotherapy, and tumor regression was readily detected soon after. A grey arrow marks the time point at which the treatment was stopped in all treatment groups, except for the one receiving late

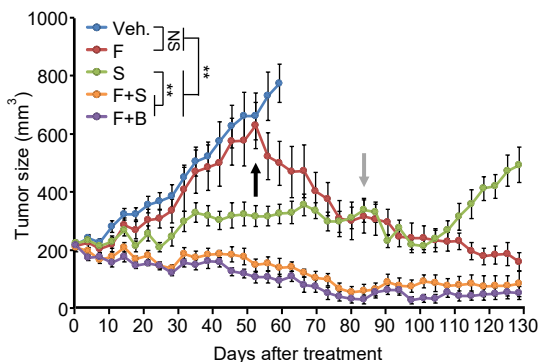


Figure 6. MEKi and fulvestrant combination induces regression of an ER⁺ NF1⁻ PDX model.

binimetinib after initial fulvestrant-monotherapy, and only the F+MEKi groups showed sustained tumor growth inhibition.

IMPACTS

Loss-of-function mutations in the *NF1* gene promote tamoxifen agonism and estrogen-deprivation resistance because neurofibromin is also a co-repressor of estrogen receptor (ER), therefore loss enhances ER transcriptional activity. While ER⁺ NF1-depleted cells are initially responsive to fulvestrant, a selective ER degrader, enhanced Ras activity promotes acquired resistance. When Ras pathway activation is inhibited with a well-tolerated MEK inhibitor, fulvestrant resistance is reversed and full tumor regression ensues. Thus, neurofibromin-depletion represents a distinct breast cancer subset where the choice of endocrine treatment may be critical, and MEK inhibitor combinations require clinical investigation. To this end, we have obtained firm pharma commitment to launch a Phase-2 clinical trial to bring this therapeutic option to patients. A role as a dual repressor for both Ras and ER may also explain the sexually dimorphic characteristics of neurofibromatosis where tumorigenesis is promoted by female puberty.

CHANGES/PROBLEMS: None.

PRODUCTS:

(1) A manuscript describing the current results has been conditionally accepted by *Cancer Cell*.

Ze-Yi Zheng, Meenakshi Anurag, Jin Cao, Burcu Cakar, Xinhui Du, Jing Li, Philip Lavere, Jonathan T. Lei, Purba Singh, Sinem Seker, Doug Chan, Xi Chen, Kimberly C. Banks, Richard B. Lanman, Maryam Nemati Shafae, Susan Hilsenbeck, Charles E. Foulds, Matthew J. Ellis^{1†}, Eric C. Chang. 2017. Neurofibromin is an Estrogen Receptor α Transcriptional Corepressor in Breast Cancer.

(2) An abstract was selected for a talk at the NF Conference held at San Francisco in 2019:

Ze-Yi Zheng, Meenakshi Anurag, Jin Cao, Burcu Cakar, Xinhui Du, Jing Li, Philip Lavere, Jonathan T. Lei, Purba Singh, Sinem Seker, Doug Chan, Xi Chen, Kimberly C. Banks, Richard B. Lanman, Maryam Nemati Shafae, Susan Hilsenbeck, Charles E. Foulds, Matthew J. Ellis^{1†}, Eric C. Chang. Neurofibromin also has a GAP-independent activity, acting as a transcriptional co-repressor for estrogen receptor-alpha.

(3) An abstract was presented at the Cell Hallmarks of Cancer Symposium held at Seattle in 2019.

Ze-Yi Zheng, Meenakshi Anurag, Jin Cao, Burcu Cakar, Xinhui Du, Jing Li, Philip Lavere, Jonathan T. Lei, Purba Singh, Sinem Seker, Doug Chan, Xi Chen, Kimberly C. Banks, Richard B. Lanman, Maryam Nemati Shafae, Susan Hilsenbeck, Charles E. Foulds, Matthew J. Ellis^{1†}, Eric C. Chang. 2017. Neurofibromin is an Estrogen Receptor α Transcriptional Corepressor in Breast Cancer.

(4) With the support of this DOD grant, we have obtained an Expansion Award from DOD that will add two additional year of support to this project to investigate NF1's role in bone metastasis.

PARTICIPANTS & OTHER COLLABORATING ORGANIZATIONS:

Name	Project role	ORCID ID	Person Mon worked	Project contribution	Funding support
Eric Chang	PI	0000-0002-1375-5088	4.2	Design and execute all the studies in Aim 1, and write the paper.	This grant.
Matthew Ellis*	Partnering PI	0000-0002-8467-8534	0.6	Design and execute the studies in Aim 2, and write the paper.	This grant.
Charles Foulds	Co-Investigator	<u>0000-0003-4908-1473</u>	0.6	Assist in the design and execution of the studies in Aim 1, and the study of the co-regulator function in particular, and write the paper.	This grant.
Seker Sinem*	Tech	N/A	6.0	Assist Dr. Ellis in the studies in Aim 2.	This grant.
Purba Singh*	Tech	0000-0002-8467-8534	3.0	Conduct animal studies under the direction of Dr Ellis in Aim 2	This grant
Zeyi Zheng	Staff Sci	0000-0001-6536-4874.	4.0	Assist Dr. Chang in the design and execution of all the studies	This grant

				in Aim 1, and supervise Ms Kenney	
Hilda Kennedy	Tech	NA.	4.0	Provide technical support on all projects.	This grant

*Personnel supported by Ellis's portion of the grant.

SPECIAL REPORTING REQUIREMENTS

None.

APPENDIX:

The paper conditionally accepted by *Cancer Cell*, which is currently awaiting final approval.

Cancer Cell

Neurofibromin is an Estrogen Receptor- α Transcriptional Co-repressor in Breast Cancer

--Manuscript Draft--

Manuscript Number:	CANCER-CELL-D-19-00499R3
Full Title:	Neurofibromin is an Estrogen Receptor- α Transcriptional Co-repressor in Breast Cancer
Article Type:	Research Article
Keywords:	Estrogen receptor; Breast Cancer; RAS; NF1; neurofibromin; endocrine therapy; GAP; transcription; GTPase; Tamoxifen; estradiol; co-repressor; co-regulator; fulvestrant; MEK inhibitor, Drosophila, yeast.
Corresponding Author:	Eric C. Chang Baylor College of Medicine Houston, Texas UNITED STATES
First Author:	Ze-yi Zheng
Order of Authors:	Ze-yi Zheng Meenakshi Anurag Jonathan T. Lei Jin Cao Purba Singh Jianheng Peng Hilda Kennedy Nhu-Chau Nguyen Yue Chen Philip Lavere Jing Li Xin-Hui Du Burcu Cakar Wei Song Beom-jun Kim Jiejun Shi Sinem Seker Doug W Chan Guo-qiang Zhao Xi Chen Kimberly C Banks Richard B, Lanman Maryam Nemat Shafae Xiang H.-F Zhang Sahas Vasaikar Bing Zhang

	Susan G. Hilsenbeck
	Wei Li
	Charles E. Foulds
	Matthew J Ellis
	Eric C. Chang
Abstract:	<p>We report that neurofibromin, a tumor suppressor and Ras-GAP (GTPase Activating Protein), is also an estrogen receptor-α (ER) transcriptional co-repressor through leucine/isoleucine-rich motifs that are functionally independent of GAP activity. GAP activity, in turn, does not impact ER binding. Consequently, neurofibromin-depletion causes estradiol hypersensitivity and tamoxifen agonism, explaining the poor prognosis associated with neurofibromin-loss in endocrine therapy-treated ER + breast cancer. Neurofibromin-deficient ER + breast cancer cells initially retain sensitivity to selective estrogen receptor degraders (SERDs). However, Ras activation does play a role in acquired SERD resistance, which can be reversed upon MEK inhibitor addition, and SERD/MEK inhibitor combinations induce tumor regression. Thus, neurofibromin is a dual repressor for both Ras and ER signaling, and co-targeting may treat neurofibromin-deficient ER + breast tumors.</p>
Suggested Reviewers:	<p>Jason Carroll University of Cambridge</p> <p>ER expert</p> <p>Donald McDonnell Duke University</p> <p>ER Expert</p> <p>Carlos Arteaga UTSW</p> <p>ER+ breast cancer expert</p> <p>Gordon Mills OHSU</p> <p>ER+ breast cancer expert</p> <p>George Sledge Stanford University School of Medicine</p> <p>Expert on ER+ breast cancer</p> <p>Michael Wigler Cold Spring Harbor Laboratory</p> <p>Ras/NF1 expert</p> <p>Dafna Bar-Sagi New York University</p> <p>Ras expert</p> <p>Bruce Korf University of Alabama at Birmingham</p> <p>NF1 expert</p>
Opposed Reviewers:	<p>Myles Brown Dana Farber Cancer Institute</p> <p>Potential conflict of interest</p>
Additional Information:	

Question	Response
<p>If your paper is accepted, we encourage you to publish the original, unprocessed data alongside your Cell Press paper through Mendeley Data. For more information, please refer to our detailed instructions.</p>	<p>I do not wish to publish my original data.</p>



CANCER PREVENTION & RESEARCH
INSTITUTE OF TEXAS



LESTER & SUE SMITH
BREAST
CENTER

Matthew J. Ellis, MB., BChir., Ph.D., FRCP
C. Kent Osborne Endowed Chair
Lester and Sue Smith Breast Center
CPRIT Scholar in Cancer Research
McNair Medical Institute
One Baylor Plaza, BCM 600
Houston, TX 77030
mjellis@bcm.edu
TEL: (713) 798-1845
FAX: (713) 798-1642

January 9th, 2020

Dear Dr. Turk,

Thank you very much for the thoughtful guidance. We have chosen to take the option of publishing the paper without the ER CHIP-seq data. In turn, we added more qPCR validation such that the ERE sites bound by ER (Figure 2C) can match those bound by NF1 (Figure 5C), which we believe strengthens the paper.

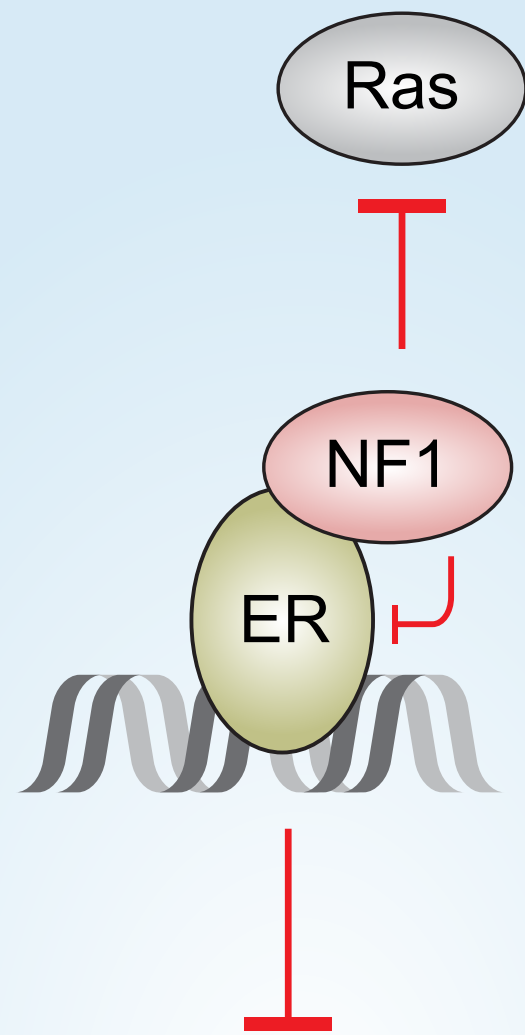
Sincerely,

Matthew J. Ellis, MB., BChir., Ph.D., FRCP
C. Kent Osborne Endowed Chair
Director, Lester and Sue Smith Breast Center

Eric Chang, PhD
Associate Professor
Lester and Sue Smith Breast Center

Our response to the editor is included in the cover letter

NF1 represses ER,
independent of
its GAP activity

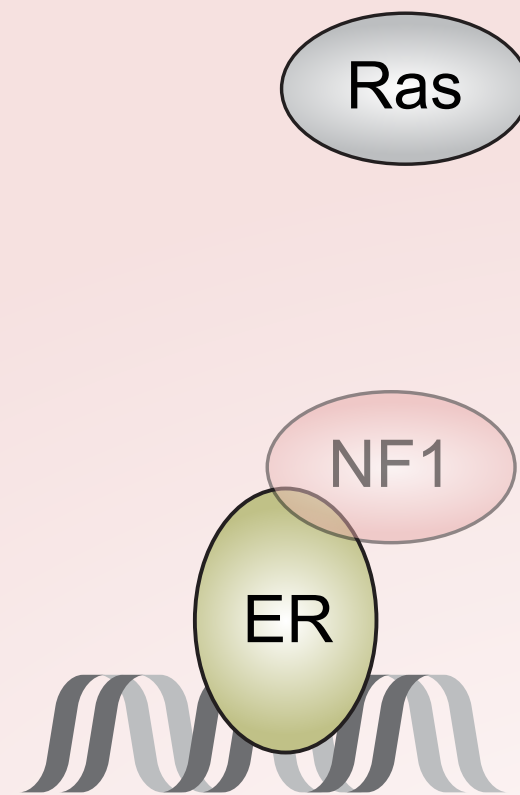


Expression of
target genes

Somatic loss
of NF1



NF1 loss enhances
transcription and
promotes treatment resistance

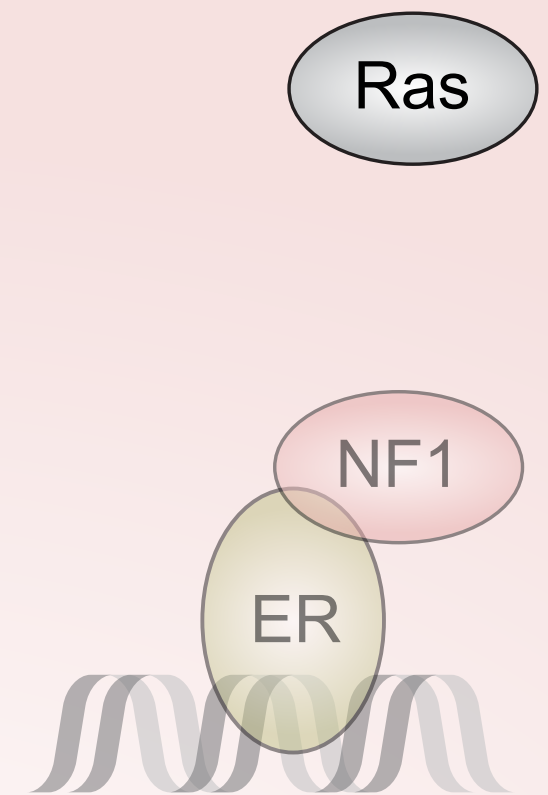
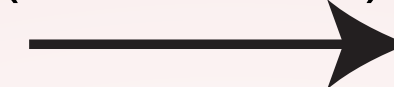


Increased expression
of target genes

Tamoxifen agonism
E2 hypersensitivity

**Tamoxifen
and
Aromatase inhibitor
resistance**

SERD
(Fulvestrant)



MEK inhibition

Tumor growth

**Acquired
SERD resistance**

Neurofibromin is an Estrogen Receptor- α Transcriptional Co-repressor in Breast Cancer

Ze-Yi Zheng¹, Meenakshi Anurag¹, Jonathan T. Lei^{1,2}, Jin Cao³, Purba Singh¹, Jianheng Peng^{1,4}, Hilda Kennedy¹, Nhu-Chau Nguyen¹, Yue Chen⁵, Philip Lavere³, Jing Li¹, Xin-Hui Du^{1,6}, Burcu Cakar¹, Wei Song¹, Beom-Jun Kim¹, Jiejun Shi¹, Sinem Seker¹, Doug W. Chan^{1,3}, Guo-Qiang Zhao⁶, Xi Chen³, Kimberly C. Banks⁷, Richard B. Lanman⁷, Maryam Nemati Shafae¹, Xiang H.-F. Zhang^{1,3}, Suhas Vasaikar¹, Bing Zhang¹, Susan G. Hilsenbeck¹, Wei Li¹, Charles E. Foulds^{3,8}, Matthew J. Ellis^{1,3,9*}, Eric C. Chang^{1,3*}

¹Lester and Sue Smith Breast Center and Dan L. Duncan Comprehensive Cancer Center, Baylor College of Medicine, USA.

²Interdepartmental Program in Translational Biology and Molecular Medicine, Baylor College of Medicine, USA.

³Department of Molecular and Cellular Biology, Baylor College of Medicine, USA.

⁴Department of Physical Examination, the First Affiliated Hospital of Chongqing Medical University, P.R. China

⁵Adrienne Helis Malvin Medical Research Foundation, New Orleans LA, USA.

⁶Department of Bone and Soft Tissue, Zhengzhou University Affiliated Henan Cancer Hospital and College of Basic Medical Sciences, Zhengzhou University, P. R. China.

⁷Guardant Health, Redwood City CA, USA.

⁸Center for Precision Environmental Health, Baylor College of Medicine, USA.

⁹Department of Medicine, Baylor College of Medicine, USA.

*These authors contributed equally. Correspondence: echangl@bcm.edu, 713-798-3519 (P) 713-798-1642 (F) and mjellis@bcm.edu, 713-798-1845 (P) 713-798-8884 (F)

Summary

We report that neurofibromin, a tumor suppressor and Ras-GAP (GTPase Activating Protein), is also an estrogen receptor- α (ER) transcriptional co-repressor through leucine/isoleucine-rich motifs that are functionally independent of GAP activity. GAP activity, in turn, does not impact ER binding. Consequently, neurofibromin-depletion causes estradiol hypersensitivity and tamoxifen agonism, explaining the poor prognosis associated with neurofibromin-loss in endocrine therapy-treated ER⁺ breast cancer. Neurofibromin-deficient ER⁺ breast cancer cells initially retain sensitivity to selective estrogen receptor degraders (SERDs). However, Ras activation does play a role in acquired SERD resistance, which can be reversed upon MEK inhibitor addition, and SERD/MEK inhibitor combinations induce tumor regression. Thus, neurofibromin is a dual repressor for both Ras and ER signaling, and co-targeting may treat neurofibromin-deficient ER⁺ breast tumors.

Significance

Loss-of-function mutations in the *NF1* gene promote tamoxifen agonism and estrogen-deprivation resistance because neurofibromin is also a co-repressor of estrogen receptor (ER), therefore loss enhances ER transcriptional activity. While ER⁺ NF1-depleted cells are initially responsive to fulvestrant, a selective ER degrader, enhanced Ras activity promotes acquired resistance. When Ras pathway activation is inhibited with a well-tolerated MEK inhibitor, fulvestrant resistance is reversed and full tumor regression ensues. Thus, neurofibromin-depletion represents a distinct breast cancer subset where the choice of endocrine treatment may be critical, and MEK inhibitor combinations require clinical investigation. A role as a dual repressor for both Ras and ER may also explain the sexually dimorphic characteristics of neurofibromatosis where tumorigenesis is promoted by female puberty.

Introduction

Germline mutations in the *NFI* (*Neurofibromatosis type 1*) gene are responsible for neurofibromatosis type 1, the most common inherited disorder that predisposes individuals to both benign and malignant tumors of the nervous system (Ratner and Miller, 2015), as well as an increased risk for breast cancer (Madanikia et al., 2012; Salemis et al., 2010; Sharif et al., 2007). Analysis of TCGA data has shown that *NFI* is mutated in a wide range of common cancers (e.g., melanoma, lymphoma, and cancers of the lung, breast, and colon) (Yap et al., 2014). Thus, *NFI*-deficiency underlies the formation and/or progression of a large number of cancers.

NFI encodes neurofibromin, an established GTPase-Activating-Protein (GAP), that attenuates Ras signaling (Maertens and Cichowski, 2014). The human genome contains up to 14 Ras GAPs that share no significant sequence homology beyond the GAP domain. However, across species there is extensive evolutionary sequence conservation outside of the relatively small GAP domain (e.g., 83% overall identity in amino acid sequence between human and salmon neurofibromins), suggesting that neurofibromin has other yet undisclosed functional domains.

Approximately 80% of breast cancers are positive for estrogen receptor- α (ER⁺), a ligand-dependent transcription factor that is activated by estradiol (E2) (Feng and O'Malley, 2014). The E2-liganded ER recruits co-activators (such as steroid receptor coactivators, SRC-1-3) to estrogen-responsive elements (EREs) in ER-regulated genes. Tamoxifen, a selective estrogen receptor modulator (SERM), is predominantly antagonistic in breast cancer cells, hence its therapeutic effect. When tamoxifen binds to ER, co-activators are displaced by co-repressors in the ER-ERE complex (Shang et al., 2000). Established ER co-repressors bind ER via their leucine/isoleucine-rich motifs, and substitutions of L or I with an A can disrupt binding (Hu and Lazar, 1999).

Interactions are also mediated by electrostatic interactions (Heldring et al., 2007; Shiau et al., 1998).

Besides tamoxifen, ER⁺ breast cancer can be treated with estrogen deprivation through ovarian suppression and aromatase inhibition (AI), and ER can be directly targeted by selective estrogen receptor degraders (SERDs), such as fulvestrant, which induce ER protein turnover. However, relapse is common, and the majority of breast cancer deaths occur after a diagnosis of an ER⁺ primary cancer. To identify driver mutations that promote tamoxifen resistance, we performed somatic mutation analysis on primary tumors accrued from patients with early stage ER⁺ breast cancer treated with adjuvant tamoxifen monotherapy and found that *NFI* nonsense and frameshift mutations were associated with a markedly higher risk of breast cancer recurrence and death (Griffith et al., 2018). This was not the case for missense mutations, and GAP-inactivating missense *NFI* mutations were extremely uncommon.

These findings provoked an investigation of GAP-independent functions of neurofibromin, with the conclusion that neurofibromin also functions as an ER transcriptional co-repressor. Neurofibromin binding to ER is mediated by co-repressor motifs that are not required for GAP activity; conversely, GAP activity does not affect ER binding. *NFI* inactivation enhances ER transcriptional activity, permitting ER⁺ breast cancer cells to grow in very low levels of E2 and also promotes the agonistic properties of tamoxifen. While *NFI*-deficient ER⁺ breast tumors are therefore likely to be resistant to both tamoxifen and AIs, they retain initial responsiveness to the SERD fulvestrant. However, in the presence of fulvestrant, the survival of these cells become dependent on Ras activity to induce acquired fulvestrant resistance, which is reversible upon addition of a MEK inhibitor and the combination induces tumor regression. Thus, we demonstrate that loss of *NFI* directly de-represses two oncogenic pathways mediated by Ras and ER, and in

preclinical models these pathways can be co-targeted to effectively treat ER⁺ *NF1*-depleted breast tumors.

Results

NF1 loss correlates with poor patient outcome in ER⁺ breast cancer. While *NF1* mutation frequencies are low in primary ER⁺ breast cancer (2% in TCGA (TCGA, 2012) as shown in Figure 1A, and 4% in our patient cohort (Griffith et al., 2018)), *NF1* mutation frequency is higher in metastatic ER⁺ breast cancer patients (n=535) (Lanman et al., 2015; Zill et al., 2018) when circulating cell-free tumor DNA was sequenced (18%, Figure 1A and Supplemental Table S1). Similar enrichment of *NF1* mutations in metastatic ER⁺ breast cancer has been reported by others (Bertucci et al., 2019; Meric-Bernstam et al., 2014; Pearson et al., 2019; Razavi et al., 2018; Sokol et al., 2019; Yates et al., 2017). These observations suggest that somatic *NF1* events are an important class of mutations driving breast cancer progression.

In our previous study, only *NF1* nonsense/frameshift mutations correlated with poor outcome after tamoxifen treatment, and no GAP-inactivating missense mutations were found. When examining the COSMIC database, a C to T nonsense mutation at R2450 (*R2450**) is the most frequent non-silent *NF1* mutation, found 28 times (Figure S1A). Nonsense/frameshift mutations can trigger mRNA degradation through nonsense-mediated decay. Consistent with this mechanism, greatly reduced full-length *NF1* mRNA levels were observed in both TCGA (Figure 1B) and METABRIC (Curtis et al., 2012) (Figure S1B) samples when nonsense/frameshift mutations were present. Similar reduction of *NF1* mRNA in tumors carrying *NF1* mutations have also been reported in another patient cohort (Pearson et al., 2019). ER⁺ breast cancer is also treated with aromatase inhibition (AI); therefore, we examined gene expression data from the ACOSOG Z1031 clinical trial, where patients were treated with an AI before surgery (Ellis et al., 2011). These data demonstrated that while a multi-gene proliferation score (MGPS) (Ellis et al., 2017) decreased after AI treatment in tumors with higher *NF1* mRNA levels, reduced suppression of

proliferation (high MGPS) was observed in tumors with low *NF1* mRNA levels, indicating AI resistance (Figure 1C and Supplemental Table S2). Finally, we found that NF1 proteins missing a small portion of the C-terminus caused by the *NF1-R2450** mutation or by two other recurrent nonsense/frameshift mutations, *NF1-R2258** and *NF1-Y2285** (Figure S1A), could not be efficiently expressed unless a proteasome inhibitor was added (Figure S1C), supporting the possibility that some C-terminally truncated NF1 proteins may be unstable.

Collectively, these findings raise the possibility that depletion of neurofibromin is a common consequence of nonsense/frameshift mutations and most associated with poor outcomes. Importantly sequencing studies have found few recurrent inactivating mutations in the NF1 GAP domain, leading us to speculate that NF1 protein may harbor additional negative regulatory functions relevant to breast cancer pathogenesis.

***NF1*-depletion promotes tamoxifen agonism and E2 hypersensitivity in ER⁺ breast cancer cells.** To investigate the consequences of *NF1*-depletion on ER⁺ breast cancer, MCF-7 ER⁺ breast cancer cells were engineered to harbor lentiviruses expressing one of two doxycycline (DOX)-inducible shRNA clones (C5 and C6). Upon DOX addition (+DOX), NF1 protein levels were reduced by ~70% as detected by a monoclonal antibody (mAb) we raised (Figure S1 D and E). Increased ERK activating phosphorylation (pERK1/2) in DOX-treated cells vs. vehicle treated or scrambled shRNA controls indicated the anticipated reduction in GAP activity (Figure S1E). An *NF1* shRNA-resistant expression construct reversed these effects (Figure S1E).

Remarkably, when *NF1* expression was suppressed (+DOX) in MCF-7 cells as well as two more ER⁺ breast cancer cell lines ZR-75B and T47D (Figure S1F), *in vitro* growth was consistently stimulated by 4-hydroxy-tamoxifen (4-OHT) under E2-deprived conditions (charcoal-stripped serum) (Figure 1D and Figure S1G), in comparison to the non-silenced control (–DOX) or the

scrambled shRNA +DOX control, indicating an *NF1* loss mediated transition from 4-OHT antagonism to agonism. Furthermore, *NF1*-silenced cells proliferated at lower concentrations of E2 than controls, and higher E2 concentrations paradoxically inhibited cell growth indicating E2 hypersensitivity (Figure 1E and Figure S1H). Two pools of *NF1* “knock-out” (KO) MCF-7 cells were independently created by CRISPR-Cas9 (Figure S1D) with results similar to the shRNA data (Figure 1 D and E). MDA-MB-231 cells are ER⁻, and *NF1* expression is barely detectable (Ogata et al., 2001) due to a frameshift mutation (*NF1-T467^{fs}*) (Neve et al., 2006). These ER⁻ “*NF1*^{low}” cells were unresponsive to 4-OHT or E2, indicating a requirement for ER for the endocrine effects of *NF1* perturbation (Figure S1 G and H). E2 hypersensitivity and 4-OHT agonism were reproduced *in vivo* using an MCF-7-based xenograft mouse model — tamoxifen stimulated the growth of *NF1*-silenced tumors (Figure 1F left), and these tumors grew at a dose of E2 (0.05 mg dose) that had almost no discernable effect on the growth of control tumors (Figure 1F, right).

NF1-depletion globally enhances ER transcriptional activity. Since the abnormal E2 and tamoxifen responses observed in *NF1*-depleted cells are ER-dependent, we investigated whether *NF1*-depletion affects ER-dependent transcription. First, the mRNA levels of established ER-target genes were examined by qPCR in MCF-7 cells, and the expression levels of *GREB1* and *pS2/TFE1* in the presence of E2 were elevated when *NF1* was depleted by DOX-inducible shRNA (Figure S2A) or CRISPR-mediated KO (Figure S2B). This increase was not due to an increase in ER protein levels and could be reversed by the shRNA-refractory *NF1* construct (“*NF1*-rescue”, Figure S2A), indicating the specificity of the shRNA targeting. Gene expression was also stimulated by 4-OHT in MCF-7 cells depleted for *NF1* by shRNA (Figure S2C) or by CRISPR (Figure S2B), consistent with conversion to agonism. E2 and 4-OHT-stimulated gene expression were similarly observed in *NF1*-silenced ZR-75B cells (Figure S2C). ER-dependent transcription

is promoted by co-activators SRC1-3, and these factors can be selectively degraded by bufalin (Wang et al., 2014). Our data showed that bufalin inhibited 4-OHT-induced enhanced gene expression in *NF1^{KD}* MCF-7 cells (Figure S2D), indicating SRC1-3 is required for this activity. Finally, we examined tumor tissues from the MCF-7 xenograft model (Figure 1E) by qPCR and found that expression of two ER target genes *GREB1* and *TFF1* was greatly enhanced when *NF1* was silenced (Figure S2E).

To examine the effects of *NF1* on gene expression in a genome-wide fashion, RNA-seq experiments were performed in control (–DOX) and *NF1* knock-down (+DOX, KD) MCF-7 cells with and without E2 stimulation. Overall, E2 altered expression from 540 genes in the control *NF1⁺* cells and 955 genes in *NF1^{KD}* cells (Figure 2A and Table S3). There was an overlap of 388 genes between the two gene sets (Table S3), indicating that expression changes of 72% (=388/540) of the observed E2-altered genes seen in *NF1⁺* cells were also altered in *NF1^{KD}* cells. These overlapping genes, referred to as the “common E2-regulon,” were analyzed by GSEA Hallmark Pathway analysis and found to be highly enriched with well-established E2-responsive genes (Figure 2A and Table S3). Furthermore, nearly all genes upregulated after E2-stimulation in *NF1⁺* cells were more strongly induced in *NF1^{KD}* cells, and the great majority of E2-repressed genes were also more strongly repressed, consistent with bidirectional ER-hyperactivity upon NF1-depletion (Zubairy and Oesterreich, 2005). The 415 (=955–540) E2-altered genes that were selectively observed in the NF1-depleted state (referred to as the “NF1^{KD}-unique E2-regulon”) were also assessed by GSEA Hallmark pathway analysis (Table S3). Aside from a predominance of additional E2-regulated genes, a K-Ras-dependent gene expression signature was also observed (Figure 2A). Gene expression changes induced by 4-OHT were also examined by RNA-seq. While 4-OHT overall displays weak agonist activity as expected (Figure S2F, Table S3), the

overlap of 4-OHT-altered gene expression between *NFI*⁺ and *NFI*^{KD} cells was 65% and enriched with well-established E2-responsive genes (Figure S2G). Furthermore, genes that were induced by 4-OHT in *NFI*⁺ cells were more highly induced, while 4-OHT-repressed genes were more strongly repressed in *NFI*^{KD} cells (Figure S2G).

To determine whether the E2-induced gene expression patterns shown in Figure 2A could be replicated in patient samples, differentially expressed genes according to *NFI* status (with or without *NFI* nonsense/frameshift mutation) in the METABRIC and TCGA ER⁺ data sets were identified, and pathway enrichments were similarly assessed (Table S4). The results were compared to the two MCF-7 E2-regulons described above. Supporting the conclusion that *NFI*-depletion dramatically affects the expression of E2-responsive genes in clinical ER⁺ specimens, E2-responsive pathway terms were most significantly modulated by *NFI* mutation status, followed by the K-Ras signature (Figure 2B). A similar conclusion has been obtained by others after examining ER⁺ breast tumors with *NFI* shallow deletion in METABRIC (Dischinger et al., 2018) and *NFI* “truncating” mutations in TCGA (Pearson et al., 2019).

***NFI*-depletion increases ER recruitment to EREs.** In the presence of E2, *NFI*-depletion mostly affects expression of known E2-responsive genes. To assess whether this is due to direct ER binding to the EREs, we performed ChIP-qPCR to analyze ER recruitment to ten well-documented ERE sites in six genes, *TFF1*, *GREB1*, *PGR*, *MYC*, *XBPI*, and *CCDN1*. The data show that *NFI*-depletion enhances ER recruitment to all of these sites (Figure 2 C and D).

In the presence of 4-OHT, expression of 542 genes was mostly detected in *NFI*^{KD} cells (Figure S2G). We examined one 4-OHT-dependent ER ChIP-seq data set (He et al., 2018) and found that 68% of these 542 genes (371/542) were also found in this ER ChIP-seq study (Table S3). All together, these data suggest that *NFI*-depletion mostly *quantitatively* enhances ER-

dependent transcription, whether it is stimulated by E2 or 4-OHT, but *NFI* loss does not substantially qualitatively alter the profile of genes that get transcribed under the experimental conditions tested.

Neurofibromin contains two leucine/isoleucine rich co-repressor motifs. Tamoxifen agonism and E2 hypersensitivity, together with the RNA-seq and ER ChIP-seq data suggested that neurofibromin may function as a ligand-dependent co-repressor for ER transcriptional activity. Consistent with this postulate, there are two consensus co-repressor motifs in neurofibromin, designated here as M1 and M2 (Figure 3A). Notably the ER binding motifs in neurofibromin family members appear to have co-evolved with emergence of estrogen-dependent reproduction. M1/2 are highly conserved in salmon, the most human-distant species examined to have an ER homolog (Rogers et al., 2000), but not in fly or yeast (Figure 3A), which do not. Furthermore, mutations affecting key residues in M1 and M2 can be found in cancer (COSMIC and METABRIC) and some of these mutations are recurrent. In particular, a somatic M1 I417M mutation was found in our patient cohort (Griffith et al., 2018), which coexisted with an *NFI* nonsense mutation suggesting a biallelic event.

The binding of ER to neurofibromin is selective, ligand-dependent, and direct. Established ER co-repressors preferentially bind to the ER ligand-binding domain (LBD) in an interaction that is enhanced by 4-OHT but not by E2 (while the reverse is the case for co-activators) (Huang et al., 2002; Shiao et al., 1998). Ligand-dependent binding of neurofibromin to the ER LBD was detected in cells using a mammalian two-hybrid assay (Chang et al., 1999), mimicking a known co-repressor NCoR1 and opposite to the behavior of the coactivator SRC-1 (Figure S3 A and B). Reciprocal co-immunoprecipitation experiments in MCF-7 and ZR-75B cells were also performed to demonstrate that neurofibromin can co-immunoprecipitate ER using our mAb and *vice versa*

(Figure S3C). NF1⁺ MCF-7 cells were used to illustrate the point that these interactions were enhanced by 4-OHT, but reduced by E2; in contrast, ER could not be pulled down in the NF1-KO line, indicating that our neurofibromin mAb is specific (Figure 3B). Finally, M2 is located in the GAP domain, which can be readily purified from *Escherichia coli* (Bollag et al., 1993). We thus determined that 4-OHT increased the efficiency of the interaction between purified NF1-M2/GAP domain and purified ER in a pull-down, confirming that the interaction between NF1 and ER is very likely direct (Figure 3C).

The human genome contains 14 potential Ras GAPs, but they do not share sequence homology beyond the GAP domain. For example, in p120GAP/RASA1, there is no identifiable M1; nor was there an M2 in a published GAP domain alignment study (Ballester et al., 1990) (Figure S3D). While ER co-immunoprecipitated NF1, ER did not co-immunoprecipitate p120/RASA1 (Figure S3C). Protein co-expression is a strong predictor for co-functionality (Wang et al., 2017a). Therefore, we assessed Gene Ontology molecular function terms of proteins whose levels positively correlated with those of neurofibromin from proteomics analysis of >100 breast cancer patient-derived samples (CPTAC) (Mertins et al., 2016). Whereas NF1 protein levels highly correlated with a number of transcription factor functionalities, and the “ligand-dependent nuclear receptor binding” term in particular, p120GAP, mostly negatively correlated with these factors (Figure S3E).

ER binding and GAP activity are two independent functions of neurofibromin. To determine whether that neurofibromin can directly interact with ER via M1/2 without a requirement for GAP activity or Ras pathway activation, we first took a pharmacological approach using Raf and MEK inhibitors, dabrafenib and trametinib (Robert et al., 2015). Here we found that Raf/MEK inhibition did not affect E2-dependent transcription measured by qPCR

in either NF1⁺ or *NF1*-silenced MCF-7 cells (Figure S3F). Immunoblotting detected substantial loss of pERK levels by dabrafenib and trametinib, suggesting the Ras-Raf pathway was efficiently inhibited in these experiments (Figure S3F). Bufalin, which promotes degradation of SRC1-3 co-activators, was the positive control for this study. One of the best-known examples of a Ras-ER interaction is phosphorylation at serine 118 (pS118) in ER by ERK after growth factor stimulation (Kato et al., 1995). However, this event seems to be context (e.g., cell type and/or culture conditions)-dependent and can be catalyzed by other kinases (Anbalagan and Rowan, 2015). We could not detect a significant increase in ER-pS118 in NF1 KO MCF-7 cells, despite strong increase in activating phosphorylation in ERK1/2 (Figure S3G). Finally, we note that the average IC₅₀ of trametinib in commonly used ER⁺ breast cancer cell lines under normal culture condition is 300 μM vs. 0.05 μM in melanoma cells (<https://www.cancerrxgene.org>). Thus, under standard culture conditions, Ras-Raf signaling is not critical for either ER-dependent gene expression or growth of E2-sensitive ER⁺ breast cancer cells.

To directly ascertain whether M1 and M2 are authentic ER-binding sites, residues I and V were substituted with A to create NF1-I417A-I418A and NF1-V1308A-V1309A. The I417M *NF1* somatic M1 mutant found in an ER⁺ breast cancer was also generated. Conversely, two NF1 GAP-inactivating mutants found in metastatic breast cancer, NF1-R1362Q (Lanman et al., 2015) and NF1-K1444R (Li et al., 2013) (Figure S3H), were created to assess whether ER repression is dependent on intact GAP activity. We confirmed that R1362Q and K1444R mutations greatly reduce the GAP activity of NF1, while the M1/2 mutations do not, by measuring pERK levels (Figure S3H).

Binding to ER (two-hybrid assay, Figure S3I) and repression of ER transcriptional activity (ERE-luciferase reporter assay (Hall and McDonnell, 1999), Figure S3J) were both greatly reduced

by M1 and M2 mutations; in contrast, the two GAP mutants bound and suppressed ER activity as efficiently as wild-type NF1. One GAP and one M1 mutant were chosen for further study by expressing them in *NF1*-depleted cells to levels comparable to endogenous neurofibromin in control cells (Figure S3K). The enhanced *GREB1* and *TFF1* expression in *NF1*-silenced cells was completely repressed by wild-type *NF1* and the GAP mutant, but only partially by the M1 mutant.

To ascertain whether ER-repression and GAP activity are two independent functions of NF1 without using ectopic overexpression, CRISPR-Cas9 mediated knock-in was used to create MCF-7 cells carrying homozygous *NF1-I417M* (M1) mutation or *NF1-R1362Q* (GAP) mutation (see Methods). The former cells had normal GAP activity, but their NF1-I417M cannot co-immunoprecipitate ER (Figure 3D). Similar to cells in which NF1 is depleted by shRNA or CRISPR, the *NF1-I417M* (ER binding) mutant cells showed abnormal endocrine responses because cell growth was stimulated by 4-OHT and low levels of E2; in contrast, the *NF1-R1362Q* (GAP) mutant behaved like wild-type cells (Figure 3E). We examined expression of two well-established ERE genes (*TFF1* and *GREB1*) by qPCR (Figure 3F) and found that their expression after E2 stimulation was greatly enhanced by the I417M mutation, which again behaved like full NF1-depletion. In contrast, the *NF1-R1362Q* mutant behaved like wild-type cells showing only a modest increase in gene expression.

While conducting the ER ChIP experiments, we noted a trend that more ER was recruited to the chromatin when NF1 was depleted even when the cells were seeded in the presence of vehicle alone (Figure 2D). Consistent with this, expression of *GREB1* and *TFF1* was significantly stronger in vehicle-treated *NF1-I417M* mutant cells than in wild-type and the *NF1-R1362Q* mutant cells (Figure 3F). To further examine these findings in a transcriptome-wide manner, cells were seeded in charcoal-stripped serum supplemented medium without adding ligand, and RNA-seq

experiments were performed (Table S5 and Figure 6G). When expression levels of genes (row Z-scores from “Log2 Transcripts per Million” values) in various cell lines were aligned to the list of E2-responsive genes as identified previously (Figure 2A), it was evident that the majority of the E2-induced genes were more highly expressed and many E2-repressed genes were more strongly repressed in the *NF1-I417M* mutant (right panel, first column, Figure 3G). Essentially, the *NF1-I417M* mutation mimicked E2-stimulation. In contrast, the *NF1-R1362Q* mutant behaved like wild-type, showing no detectable transcriptional phenotype (middle and right columns in the right panel, Figure 3G). These results clearly illustrate that ER-repression and Ras-repression are two independent activities of NF1 that are mediated by distinct structural motifs.

Ligand-stimulated nuclear accumulation of neurofibromin. For transcriptional regulation, neurofibromin must enter the nucleus. While neurofibromin is mainly cytoplasmic, nuclear neurofibromin has been previously reported in a variety of cell types including ER⁺ breast cancer cells (Beausoleil et al., 2004; Daston et al., 1992; Koliou et al., 2016; Kweh et al., 2009; Li et al., 2001; Nousiainen et al., 2006; Vandenbroucke et al., 2004). In one study, neurofibromin nuclear localization in neuronal cells was shown to be dependent on the Ran GTPase (Koliou et al., 2016). This mechanism may also operate in ER⁺ breast cancer, because neurofibromin co-immunoprecipitated with Ran in MCF-7 cells (Figure S3C). Since leptomycin-B (LMB) blocks CRM1-dependent nuclear export, MCF-7, ZR-75B, and T47D cells were treated with LMB. Cell fractionation was then used to demonstrate that nuclear neurofibromin is increased after nuclear export blockade (Figure 4A). We further investigated whether NF1 nuclear levels are also affected by E2. Nuclear neurofibromin was decreased by E2 but increased by 4-OHT, indicating that ligand-regulated modulation of nuclear levels is an aspect of the co-repressor function of neurofibromin (Figure 4B). 4-OHT-enhanced ER and neurofibromin co-immunoprecipitation can

be readily detected in nuclear extracts, and the percentages of co-immunoprecipitated proteins were higher in the nuclear extracts than in whole cell extracts (Figure 3B). To investigate neurofibromin subcellular localization by microscopy, an immunostaining protocol (Figure 4C) was developed using a set of cell lines with varying degrees of *NF1* expression as controls (Figure S4), which included NF1-KO cells. Two cell lines were then chosen to confirm by microscopy the impact of LMB and ER ligands on nuclear neurofibromin levels (Figure 4 D and E). Overall these results suggest that while neurofibromin is mostly cytoplasmic at steady state, it is shuttled in and out of the nucleus, possibly by Ran and CRM-1, in a manner controlled by ER ligand exposure.

Ligand-dependent association of neurofibromin with the ER-ERE complex. When E2 is present, E2-liganded ER recruits co-activators to the ERE; 4-OHT, in turn, displaces co-activators with co-repressors in the complex. These ligand-mediated actions can be recapitulated by a cell-free assay using HeLa cell nuclear extract (Foulds et al., 2013), which does not have endogenous ER. When purified recombinant ER, biotinylated ERE, and HeLa nuclear extract were combined, the E2-liganded ER-ERE complex could more efficiently pull down the co-activator SRC-1 by streptavidin beads, while NF1, like the co-repressor HDAC1, was more strongly recruited to the ER-ERE complex in the presence of 4-OHT (Figure 5A). To assess whether neurofibromin is recruited to endogenous EREs in a ligand-dependent manner, we performed CHIP-qPCR using two separate polyclonal neurofibromin antibodies, one of which, Ab-2, was generated by us (Figure S5A), and found that neurofibromin was more efficiently recruited to the EREs of *GREB1* and *TFF1* when 4-OHT, but not E2, was added (Figure S5B). NF1-KO cells were examined as the control to show antibody specificity and neurofibromin-dependency (Figure 5B). We then selected ten well-documented ERE sites in six genes, *TFF1*, *GREB1*, *PGR*, *MYC*, *XBPI*, and *CCDN1*, and

performed three separate neurofibromin ChIP-qPCR experiments to show that neurofibromin recruitment to these sites was enhanced by 4-OHT; in contrast, no neurofibromin recruitment was detected in other regions (Carroll et al., 2005; Carroll et al., 2006) that do not contain an ERE (Figure 5C). Together, these results demonstrate that neurofibromin is an authentic ER co-repressor that localizes with ER on an ERE. These findings may explain the recent observation that *NF1* loss (e.g., by loss of heterozygosity) and *ESR1* activating LBD mutations are mutually exclusive (Sokol et al., 2019), because they both lead to enhanced ER transcriptional activity (Gates et al., 2018; Jeselsohn et al., 2018).

Co-targeting Ras and ER to treat NF1-deficient ER⁺ breast tumors. The clinical and functional data presented thus far suggests that *NF1*-deficient ER⁺ breast tumors will not be effectively treated with tamoxifen or AI. However, when *NF1* was depleted by either shRNA or CRISPR, the resulting MCF-7 cells were still sensitive to the SERD fulvestrant (Figure S6A). Similar observations were made in *NF1^{KD}* ZR-75B and T47D cells (Figure S6B). However, in *NF1*-silenced MCF-7 cells fulvestrant produced an enhanced compensatory activation of the Ras-Raf-MEK-ERK pathway that may promote cell survival and/or drug resistance in spite of effective ER inhibition (Figure 6A). Thus, combinatorial targeting of both ER with fulvestant and the Ras-Raf pathways was assessed to determine if NF1-deficient ER⁺ breast cancer can be effectively treated with this strategy. *In vitro*, the combination of Raf and MEK inhibitors, dabrafenib and trametinib enhanced fulvestrant activity to inhibit cell growth by mostly increasing apoptosis in *NF1^{KD}* MCF-7 and ZR-75B cells (Figure S6C). Immunoblots showed that all drugs inhibited the intended targets (Figure 6A). To develop a clinical protocol, we next investigated whether the dabrafenib and trametinib combination could be replaced by a single MEK inhibitor (MEKi). Selumetinib is a new generation MEKi that is less toxic than trametinib due to a shorter half-life

is under consideration by the FDA for the treatment of plexiform neurofibromas in pediatric patients with neurofibromatosis (Dombi et al., 2016; Gross et al., 2018). Our data demonstrate that *in vitro*, fulvestrant plus selumetinib also strongly inhibited cell growth and induced apoptosis in *NF1*-silenced MCF-7, ZR-75B, and T47D cells whereas single agent exposure did not (Figure 6B). Immunoblotting was performed to confirm that the drugs effectively target ER and ERK activation (Figure 6A and Figure S6D).

In vivo, while tumors from the MCF-7 *NF1^{KD}* xenograft model (+DOX) initially responded to fulvestrant, at later time points these tumors acquired resistance (Figure S6E). Acquired fulvestrant resistance in *NF1*-depleted ER⁺ breast cancer cells has recently also been reported by others (Pearson et al., 2019). We further demonstrated that the fulvestrant-resistant tumor outgrowth in ER⁺ *NF1^{low}* cells *in vivo* can be blocked by dabrafenib and trametinib (Figure S6E). In addition, RNA-seq (Li et al., 2013) and mass spectrometry data (Huang et al., 2017) suggested that a patient-derived xenograft (PDX), WHIM16 (Li et al., 2013), is *NF1*-deficient. Immunoblotting confirmed *NF1* protein levels were barely detectable in WHIM16 (Figure S6F). This PDX line was derived from a patient who died after the development of resistance to multiple lines of endocrine therapies, including fulvestrant and AI.

An initial *in vivo* assessment of dabrafenib-trametinib in WHIM16 suggested activity for Ras-dependent kinase inhibition with fulvestrant over that observed for fulvestrant alone (Figure S6F), but longer term exposure was limited by weight loss and diarrhea. We therefore replaced the dabrafenib-trametinib combination with selumetinib-laced chow and conducted a four-arm study to compare single agent efficacy versus the combination. These data demonstrate that when selumetinib was combined with fulvestrant, efficient and long-term inhibition/regression of tumor was achieved (Figure 6C) without weight loss (Figure S6H) despite only 50% inhibition of ERK

activity. In contrast, selumetinib alone slowed growth but did not induce tumor regression. Western blot confirmed ER degradation by fulvestrant and pERK inhibition by selumetinib (Figure 6D). Selumetinib did not reduce ER phosphorylation at S118 (Figure S6G), suggesting the MEKi efficacy cannot be easily explained on this basis. Binimetinib, another shorter half-life and better tolerated MEKi (Trojaniello et al., 2019), also efficiently inhibited tumor growth when combined with fulvestrant (Figure 6 C and D). Furthermore, while fulvestrant was ineffective as a single agent, fulvestrant-treated tumors regressed with later addition of binimetinib, mimicking the treatment of ER⁺ NF1^{low} tumors progressing on fulvestrant monotherapy (Figure 6C). Expression of several ERE-containing genes in treated tumors was examined by qPCR. Overall the lowest level of expression correlated with combination fulvestrant and MEKi exposure (Figure 6E).

Discussion

This study presents comprehensive evidence that neurofibromin is a transcriptional co-repressor of ER in ER⁺ breast cancer, independent of its GAP activity. Consequently, when *NFI* is depleted through somatic mutation, ER function is enhanced, leading to tamoxifen agonism, estradiol hypersensitivity, AI resistance, and poor outcome. These data suggest that the NF1-depleted ER⁺ breast cancers represent a distinct molecular subset of the disease that will require the development a new standard of care since tamoxifen is likely contraindicated and aromatase inhibition ineffective.

Our data suggest that in most cases, complete loss of the NF1 protein is responsible for enhanced ER transcriptional activity and endocrine therapy resistance. Such an *NFI-null* or *NFI^{low}* state can be caused by nonsense and frame shift mutations due to nonsense mRNA decay and/or protein instability. Although nonsense and frame shift mutations are detectable by ctDNA sequencing on metastatic patients, *NFI*-depletion can also be caused by mechanisms not detectable by targeted sequencing. In a study of breast cancer by whole genome sequencing (Nik-Zainal et al., 2016), Nik-Zainal et al have described a wide range of structural variations affecting the *NFI* gene (tandem duplications, deletions, translocations, and inversions). Furthermore, in METABRIC database *NFI* nonsense and frame shift mutations are also usually associated with shallow deletion (Griffith et al., 2018), suggesting biallelic loss of function events.

Human and salmon NF1 protein sequences share over 80% identity, which extends well beyond the GAP domain. However, defining a GAP-independent activity in neurofibromin has been difficult because of the broad range of cellular functions influenced by Ras. In hindsight, the commonly used ER⁺ breast cancer cells are ideal for investigating GAP-independent activities of neurofibromin because under standard culture conditions (e.g., in the absence of fulvestrant)

growth and ER-dependent transcription operate independently of Ras. This is consistent with the observation that oncogenic mutations in *RAS*, *RAF*, *MEK*, and *ERK* almost never occur in primary ER⁺ breast cancer. However, Ras dependent cell survival becomes evident when the ER-dependent growth is inhibited by fulvestrant. Activation of Ras is made more efficient by *NF1* loss, and *NF1*^{low} cells appear to most addicted to this pathway for survival when ER activity is efficiently inhibited. *In vivo* acquired fulvestrant resistance modeled in the NF1-depleted MCF-7 tumors, was efficiently inhibited by dabrafenib + trametinib. WHIM16 represents metastatic ER⁺ breast cancer that already had acquired fulvestrant resistance when the tumor was accrued from the patient. Fulvestrant has little effect on tumor growth unless the MEK was co-inhibited.

As ER⁺ *NF1*^{low} breast cancer acquires fulvestrant resistance, ER and MEK/ERK cross-talk likely occurs, but the finer details of this mechanism are beyond the scope of this paper. We investigated ER phosphorylation at S118 because this can be directly catalyzed by ERK. However, we could not detect a clear increase in pS118 levels in NF1-KO MCF-7 cells; conversely, in the presence of a MEKi, no decrease in pS118 can be seen in the WHIM16 tumors. Interpretation of WHIM16 experiments is complicated by the presence of fulvestrant, which greatly lowers total ER levels. There is a potential for selective stabilization of the S118 phosphorylated form of ER by other protein kinases, such as GSK3 (Grisouard et al., 2007).

In our experiments, estrogen deprivation therapy is mimicked by incubating cells in charcoal-stripped serum-containing media, as is customary in the field (Martin et al., 2017). We demonstrate that growth-simulation can be observed in *NF1*-depleted cells *in vitro* with as little as 10⁻¹² M E2 (Figure 1E), which parallels E2 levels seen in AI-treated patients. We also present evidence from a neoadjuvant trial that AI-resistance can be seen in *NF1*^{low} tumors defined at the mRNA level (Figure 1C).

Our data suggest that the majority of the 569 *NF1^{KD}*-unique genes are well-established E2-responsive genes. We speculate that the reason the expression of these genes was not readily detected unless NF1 is depleted is due to the low E2 concentration (10^{-11} M, see Methods) used to stimulate gene expression in this experiment. This E2 concentration was chosen because it best differentiates the growth of NF1⁺ from *NF1^{KD}* cells (Figure 1E), making it possible to more easily detect the differences in gene expression pattern we display. However, 10^{-11} M E2 is typical for the postmenopausal state and therefore may be too low to affect expression of some E2-responsive genes, until a co-repressor (NF1) is depleted. Of interest, the 569 genes also include genes responsible for EMT, a phenomenon that has also been seen in other resistance settings, i.e. the presence of ER-mutants (Jeselsohn et al., 2018) and ER-fusions (Lei et al., 2018). In conclusion, the majority of the genes whose expression is enhanced by NF1-depletion are authentic ER-regulated genes.

The expression of the rest of the “NF1 knock-down only” genes that do not harbor an ERE is harder to decipher, and many of these genes appear in more than one functional category (Table S3). Ras does not directly regulate gene expression, so any gene expression influenced by Ras activity is likely to be context-dependent. Of the twelve “K-RAS signaling up genes” (Table S3), three (*ID2*, *SERPINA3*, and *PCP4*) are also defined as “Estrogen response late,” so only the remaining 9 genes may be controlled by Ras activation.

In experimental systems, fulvestrant-resistance can be efficiently inhibited by further targeting MEK in both the MCF-7 and WHIM16 mouse models. These results strongly suggest that activation of the Ras-Raf pathway is the major driver for fulvestrant-resistance in NF1-deficient ER⁺ breast cancer. On this basis there is adequate clinical rationale to activate a clinical

trial of a MEKi and a SERD specifically in patients with evidence for a loss of NF1 due to somatic mutation. Of note, WHIM16 regression was achieved with a well-tolerated dose of short half-life MEKi that inhibited ERK signaling by only 50%. This suggests that long term exposures to lower dose MEKi necessary for management of advanced breast cancer will be feasible, and the pediatric experience of neurofibromatosis-related plexiform neurofibroma treatment is relevant here (Gross et al., 2018). We note that a fulvestrant and selumetinib combination failed in a randomized Phase 2 trial (23 patients per arm) in unselected postmenopausal patients (Zaman et al., 2015). This study does not exclude a benefit in ER⁺ NF1^{low} tumors, however, as it is likely that less than 5 patients harbored NF1^{low} tumors in this study. Since the prevalence of ER⁺ advanced breast cancer in the USA exceeds 100,000 patients, the ctDNA based evidence suggest at least 7,000 to 10,000 of these individuals will have an *NF1*^{low} tumor where a SERD/MEKi combination could be beneficial.

Further research may connect the ER hyperactivity induced by NF1 depletion to other paradoxical or unexplained observations in ER⁺ breast cancer, for example, regression of endocrine therapy-resistant ER⁺ breast cancer with estradiol treatment (Ellis et al., 2009). Additionally, the role of neurofibromin as an ER co-repressor may underlie the sexually dimorphic features of neurofibromatosis, including tumor growth and the preponderance of optic chiasm gliomas during female puberty (Diggs-Andrews et al., 2014).

Acknowledgements

We thank Bert O'Malley, Anna Malovannaya, and Jun Qin for the creation and maintenance of NURSA and conceptual guidance in the study of ER, Dominic Esposito and the NCI RAS Initiative at Frederick National Laboratory for Cancer Research (FNLCR) for help with NF1, and Gary Chamness for reading the manuscript. We are also thankful to Laura Smithson and David Gutmann for the technical assistance and discussion, to Daniel Yan, Khushboo Shah, Jianhui Yao, Svasti Haricharan, and Angela D. Wilkin for technical assistance, and to Ching-Yi Chang and Donald McDonnell for assistance in the two-hybrid assay. This project was assisted by the following core facilities in the Dan L. Duncan Comprehensive Cancer Center: Cell-Based Assay Screening Service, Cytometry and Cell Sorting, Biostatistics and Informatics Shared Resource, Integrated Microscopy Core, Genomic and RNA Profiling Core, and the Protein and Monoclonal Antibody Production Shared Resource, which are all supported by a P30 Cancer Center Support Grant from NCI (CA125123). The Integrated Microscopy Core is also supported by grants from NIH (DK56338), CPRIT (RP150578 and RP170719) and the John S. Dunn Gulf Coast Consortium for Chemical Genomics. The Cell Sorting Core was also supported by P30AI036211 and S10RR024547. We thank all core directors and their staffs for the help. BC was supported by an ASCO Gianni Bonadonna Research Fellowship, and JTL was supported by T32GM008129 and T32CA203690 from NIH. CEF and YC were supported by the Adrienne Helis Malvin Medical Research Foundation through its direct engagement in the continuous active conduct of medical research in conjunction with BCM. ECC was supported by The Susan G. Komen Foundation (SAC150059), DOD (W81XWH-16-1-0538 and W81XWH-19-1-0527), Nancy Owen Memorial Foundation, NIH (R21CA185516 and P50CA186784), William and Ella Owens Foundation, and CPRIT (RP180844). MJE is a CPRIT Scholar in cancer research and was

supported by CPRIT Established Investigator Recruitment Award RR140033, R01 CA095614, and Susan G. Komen for the Cure Promise Grant PG12220321.

Author contribution: ZYZ, MJE, and ECC are responsible for the design, analysis, and overall execution of the experiments. ZYZ, MA, JC, PS, JP, JTL, NCN, PL, YC, JL, XD, BC, HK, WS, BJK, JS, SS, DWC, CQZ, XC, KCB, RBL, MNS, XHFZ, SV, WL, BZ, CEF, and SGH conducted the experiments and/or data analysis. The paper was mostly written by ZYZ, MJE, and ECC and reviewed by all authors.

Author information: For reprints and permission, information is available at www.nature.com/reprints. Most authors declare no competing financial interests except: KCB and RBL are stockholders and employees of Guardant Health, Inc., CEF discloses an equity position in Coactigon, Inc., and MJE received consulting fees from Abbvie, Sermonix, Pfizer, AstraZeneca, Celgene, NanoString, Puma, and Novartis, and is an equity stockholder, consultant, and Board Director member of BioClassifier, and inventor on a patent for the Breast PAM50 assay.

Correspondence and requests for materials should be addressed to echang1@bcm.edu or mjellis@bcm.edu.

Figure legends

Figure 1. *NF1* loss promotes tamoxifen agonism and E2 hypersensitivity leading to poor patient outcome in ER⁺ breast cancer. **A.** The percentages of ER⁺ primary vs. metastatic breast cancers carrying *NF1* mutations were analyzed by Fisher Exact test. NS and FS stand for nonsense and frameshift, respectively. The number of patients carrying a particular type of *NF1* mutation is shown at the upper left side of each column. **B.** Boxplot analysis of *NF1* mRNA levels in ER⁺ breast tumors carrying different *NF1* mutations in the RNA-seq database of TCGA. *P*-value by Wilcoxon rank sum test. **C.** Patient samples were stratified by *NF1* mRNA levels according to TCGA definitions of high vs. low expression (Mean – 1.5 × SD). The Boxplot shows comparison of multigene proliferation score (MGPS) in tumors before treatment (BT) and on treatment (OT) by AI. The differences in MGPS before and during treatment in each *NF1* group were analyzed by the Wilcoxon signed-rank test. The differences in MGPS as a result of treatment between the two *NF1* groups were further analyzed by Wilcoxon rank sum test (p value marked in red). **D.** DOX-inducible gene silencing using lentiviral *NF1* shRNA clone C5 (dotted lines) and CRISPR-mediated *NF1*-KO (solid line) were performed in MCF-7 cells. NF1⁺ cells in these experiments (–DOX for shRNA or the scrambled gRNA control for the CRISPR-KO) are marked in blue, while NF1-depleted cells (+DOX for shRNA and KO cells) are marked in red, and the two KO clones are further differentiated by open and closed circles. These cells were seeded in E2-deprived medium, to which 4-OHT at indicated concentrations was added. Cell numbers were measured 6 days later. Experiments were conducted as biological triplicates (n = 3 experiments), except for MCF-7 cells carrying *NF1* shRNA C5 (n = 8 experiments). See Figure S1G for scrambled shRNA and clone C6 of shRNA targeting *NF1*. **E.** Cell growth in response to E2 was similarly analyzed as in panel-D. n = 3 experiments, except for MCF-7 cells carrying *NF1* shRNA C5 (n = 8

experiments). **F.** MCF-7 cells carrying DOX-inducible *NFI* shRNA were transplanted into the mammary fat pads of ovariectomized nude mice, supplemented by an E2-capsule. When tumors appeared, the original E2-capsule was removed, and the resulting mice were randomized into two sets (DOX or vehicle treated). Each set was then treated by either tamoxifen (5 mg/mouse, left), or E2 (at indicated doses, right). For *NFI*⁺ tumors, n=10, 12, 12, and 8 mice per group for treatment of vehicle, 0.05 mg E2, 0.5 mg E2, and tamoxifen; for *NFI*^{KD} tumors, n = 10, 13, 11, and 8 mice per group. The inset shows *NFI*-silencing validation by qPCR 2 weeks post-DOX addition. Data are reported as mean±SEM. *p<0.05, **p<0.01 by pair-wise two-tailed Student's t-test, unless otherwise indicated.

Figure 2. *NF1*-depletion globally enhances ER transcriptional activity. **A.** RNA-seq was performed on $NF1^+$ or $NF1^{KD}$ MCF-7 cells treated with E2 or vehicle. A Venn diagram depicts the number of E2-mediated differentially expressed genes in $NF1^+$ (red) vs. $NF1^{KD}$ cells (blue) and those that overlap (“common E2-regulon,” purple). The common E2-regulon genes identified in $NF1^+$ and $NF1^{KD}$ cells were ranked by (Log₂) fold-change in gene expression, and enrichment for Hallmark Pathways by GSEA is shown to the right (red line marks an FDR cutoff at 0.05). GSEA analysis was also performed to examine Hallmark Pathways selectively enriched in $NF1^{KD}$ cells (“ $NF1^{KD}$ unique E2-regulon”). **B.** Genes identified in panel-A were also examined in the TCGA and METABRIC ER⁺ breast cancer cases to identify those genes that are differentially expressed (Table S4) between tumors with wild-type *NF1* and *NF1* frameshift/nonsense mutations. The enriched Hallmark Pathways in the patient data are presented along with the results of the two E2-regulons identified in MCF-7 cells to demonstrate high degrees of functional overlap similarity between cell line and clinical datasets. **C.** ER was immunoprecipitated from cross-linked $NF1^+$ or $NF1^{kd}$ MCF-7 cells treated by E2 or vehicle, and ChIP-qPCR was performed to measure ER occupancy. Two previous known ERE-negative regions (Carroll et al., 2005; Carroll et al., 2006) were assessed as negative controls. n = 2 ChIP experiments. **D.** ER ChIP-qPCR fold-enrichment values from all ten ERE sites examined in panel-C were averaged and compared in $NF1^+$ vs. $NF1^{KD}$ (+DOX) cells seeded with or without added E2. *p<0.05, **p<0.01, and ***p<0.001 by pair-wise two-tailed Student’s t-test (n=10 sites).

Figure 3. Neurofibromin binding to ER is selectively mediated by co-repressor motifs. A. Protein alignment was created by ClustalW (MUSCLE). *NF1* has two potential co-repressor motifs, M1 and M2 (potential consensus sequences shown at the bottom). Mutations found in

cancers (COSMIC) or neurofibromatosis are colored blue, and the numbers in parentheses are the number of times found in the COSMIC database. **B.** Parental MCF-7 or the NF1-KO (clone #1) MCF-7 cells were grown in E2-deprived medium to which E2, 4-OHT, or vehicle was added. Whole cell or nuclear extracts were immunoprecipitated with NF1 or ER antibody, and the resulting samples were analyzed by immunoblotting. The number below the blot shows the percentage of co-immunoprecipitated protein. **C.** Left, recombinant purified ER- α preincubated with E2, 4-OHT, or vehicle was pulled-down by amylose beads containing His-MBP-tagged NF1-M2/GAP domain, or His-MBP-GST control, and the results were analyzed by immunoblotting. **D.** Left, whole cell lysates from parental MCF-7 cells (WT) or from a CRISPR “knock-in” mutant carrying either a *I417M* (colored red) or a *R1362Q* (colored blue) mutation grown in full-serum medium were examined by immunoblotting to measure the pERK/total ERK ratios (below). Right, reciprocal co-immunoprecipitation experiments in the presence of 4-OHT similar to those in panel-B assessed ER binding to various NF1 proteins. **E.** Parental or NF1 mutant cells were examined for cell growth in response to E2 or 4-OHT as in Figure 1. n=3 experiments. **F.** *GREB1* and *TFF1* mRNA levels from parental or NF1 mutant cells treated with vehicle or E2 were measured by qPCR (n = 3 independent experiments). Expression levels were normalized to those of vehicle-treated wild-type cells. Data are reported as mean \pm SEM. *p<0.05, **p<0.01 by pair-wise two-tailed Student’s t-test. **G.** mRNAs from cells seeded in charcoal-stripped serum were analyzed by RNA-seq. “E2-responsive genes” as defined in Figure 2A is shown on the left to which expression levels of genes (row Z-scores from “Log2 Transcripts per Million” values) in various strains were aligned.

Figure 4. ER ligand-mediated nuclear accumulation of neurofibromin. **A.** Left, whole cell lysates from indicated cell lines treated with LMB were separated into nuclear (Nu.) and cytoplasmic (Cyt.) fractions. NF1, histone-3 (nuclear marker), and GAPDH (cytoplasmic marker) were examined by immunoblotting. NF1 levels in the cytoplasmic fraction (light blue) and the nuclear fraction (red) were normalized to GAPDH and histone-3, respectively, and the sum of these two fractions is defined as total NF1 (100%). The numbers in the graph represent the percentages of NF1 determined to be nuclear. The pair-wise comparisons were between NF1 nuclear fractions. $n = 2$ experiments. **B.** Left, Cells after ligand stimulation were similarly analyzed as in panel-A and an immunoblot of treated MCF-7 cells is shown as an example. $n = 3$ experiments. **C.** Immuno-fluorescence deconvolution microscopy was performed using our monoclonal NF1 antibody on cells with varying degrees of NF1 protein. A single focal plane across the middle of the nucleus is shown. DAPI marks the nucleus. Scale bar = 20 μm . **D.** Cells treated with LMB (panel-A) were also similarly examined by microscopy. NF1 nuclear fractions were quantified in multiple cells (n). **E.** Cells after treatment with ER-ligands were similarly examined and quantified by microscopy. Data are reported as mean \pm SEM. * $p < 0.05$, ** $p < 0.01$, *** $p < 0.001$ by pair-wise two-tailed Student's t-test.

Figure 5. Ligand-dependent association of neurofibromin with the ER-ERE complex. A. Ligands were added to the HeLa S3 nuclear extract together with purified ER and biotinylated ERs immobilized onto streptavidin beads. After wash, the proteins bound to ERs with ER were analyzed by immunoblotting (left) and quantified (right). n = 4 experiments. **B.** ChIP-qPCR experiment was performed using NF1 antibody Ab-2 to assess NF1 occupancy at the ERs in *GREB1* (Region 2, Figure 2C) or *TFF1* (Region 1, Figure 2C) in parental or NF1-KO (clone 1) MCF-7 cells treated by 4-OHT. An ERE-negative regions (site 2) (Carroll et al., 2006) was also analyzed as negative control. n = 2 experiments. **C.** NF1 occupancy at the same sites as Figure 2C was validated by qPCR (n=3 separate ChIP experiments). Data are reported as mean±SEM. *p<0.05, **p<0.01, ***p<0.001 by pair-wise two-tailed Student's t-test.

Figure 6. Co-targeting Ras and ER to treat NF1-deficient ER⁺ breast cancer. **A.** MCF-7 cells were seeded in 10^{-11} M E2 to which fulvestrant, dabrafenib, trametinib or selumetinib were subsequently added at 10^{-9} , 10^{-6} , 10^{-7} or 10^{-6} M, respectively. After 6 days, proteins were measured by immunoblotting, and phosphorylation levels (as defined by the levels of the phosphorylated form over total protein) relative to the vehicle-treated cells were set to 1. We note in charcoal-stripped serum, baseline induction of pERK is weak even when NF1 is depleted. **B.** Top: cells were seed in the presence of 10^{-11} M E2 and 10^{-9} M fulvestrant, to which increasing concentration of selumetinib was added and cell numbers were measured 6 days later. $n = 3$ experiments. Bottom: the cells were treated similarly except 10^{-6} M selumetinib was used and apoptosis was measured 6-day post-treatment. We note that drug concentrations were selected such that fulvestrant plus the selumetinib combination can more easily produce an effect on the cells that is greater than either group alone. $n = 2$ experiments. **C.** WHIM16 tumors were transplanted into cleared mammary fat pad of mice and later randomized to receive treatment ($n=15$ per treatment arm) when tumor volumes reached 200 mm^3 . Tumor volume comparison was performed at 7.5-week post-treatment, and at this time point binimetinib was added to the fulvestrant-only arm (marked by the red arrow) to induce efficient tumor growth inhibition. **D.** WHIM16 tumors from each treatment arm at week-4 post-treatment (Panel-C) were analyzed by immunoblot (one representative tumor shown on the left) to assess impacts on drug targets, and the results were quantified on the right ($n = 3$ tumors). **E.** qPCR was performed to analyze expression levels of indicated genes from the same tumor samples as in panel-D. Data are reported as mean \pm SEM. * $p < 0.05$, ** $p < 0.01$ by t-test.

STAR★METHODS

LEAD CONTACT AND MATERIALS AVAILABILITY

Further information and requests for resources or reagents should be directed to the lead contact Dr. Eric C. Chang at echang1@bcm.edu.

EXPERIMENTAL MODEL AND SUBJECT DETAILS

Cell lines

The human cell lines, growth media, and general methods of cell culture have been previously reported (Zheng et al., 2015), unless otherwise indicated. All lines were routinely tested for mycoplasma contamination. Estrogen deprivation was achieved by seeding cells in phenol red-free media (DMEM for ZR-75B and RPMI1640 for MCF-7 and T47D cells) containing 10% charcoal-stripped fetal bovine serum (Sigma-Aldrich) for two days prior to the experiment.

The procedures for producing lentivirus, infecting breast cancer cells, and selecting for stable integrants were also conducted as previously described (Zheng et al., 2015). The cells stably expressing inducible shRNA were collected using FACS (Aria II, Becton Dickinson) two days after DOX treatment (2 $\mu\text{g/ml}$) by examining the presence of turboRFP, which is expressed together with the shRNA from the same bicistronic transcript. Typically, >85% of transduced cells were RFP⁺. For *NFI* overexpression and CRISPR-mediated knock-out by two gRNA sequences, cells were transduced and selected in puromycin (1 $\mu\text{g/ml}$) and pooled.

Animals

All animal work was approved by the Baylor College of Medicine Institutional Animal Care and Use Committee. For MCF-7 xenografts, prior to transplantation, 5-6 week old female

nude mice (Envigo International) were ovariectomized and left to recover for two weeks before an estrogen “capsule” (Robinson and Jordan, 1989) (0.7 cm silicone tubing, Dow Corning) was inserted. These capsules contain 0.5 mg E2 mixed with silicone gel (Factor II) to keep the final weight of the filler at 2 mg. Three days later, one million human cancer cells were suspended in Growth Factor-Reduced Matrigel (BD Biosciences) and PBS and injected into the No. 9 mammary glands. When average tumor volume reached $\approx 200 \text{ mm}^3$, the mice were randomized into different treatment groups, and the E2 capsule in the tumor-bearing mice was replaced with a fresh one, or with a tamoxifen pellet (5 mg/pellet, Innovative Research of America). DOX was added in the drinking water at 0.2 mg/ml to silence *NFI* expression. For PDX studies, WHIM16 tumors were engrafted into cleared mammary fat pads of SCID/bg female mice (Envigo International) and allowed to grow without exogenous E2 supplementation until tumors reached $\approx 200 \text{ mm}^3$. Mice were then randomized into different treatment groups. Fulvestrant was injected subcutaneously at 250 mg/kg weekly. Trametinib (1 mg/kg), dabrafenib (30 mg/kg), binimetinib (20 mg/kg), and selumetinib (20 mg/kg) were given daily as chow (Research Diets Inc.). Mouse body weight was measured twice weekly to monitor treatment toxicity.

METHOD DETAILS

Chemicals

Chemicals used are listed in Key Resource Table. Note that with the exception of the animal experiments, in all other experiments involving E2, the water-soluble version was used. Ethanol was used to dissolve 4-OHT, while DMSO was used to dissolve trametinib, dabrafenib, fulvestrant, and selumetinib.

Plasmids

Scrambled and *NF1*-targeting shRNAs (clone C5 and C6) in pGIPZ were obtained from Dharmacon. All nucleotide sequences used in this study are described in Key Resource Table. The shRNA clones were subcloned into pINDUCER11, with which cell lines stably expressing DOX-inducible scrambled or *NF1* shRNA were later created as described (Zheng et al., 2015). Unless otherwise mentioned, data obtained from cell lines expressing *NF1* shRNA C5 are shown in the figures, while the cells expressing C6 were also tested in most experiments. *NF1* CRISPR-Cas9 knock-out (KO) constructs (clone #1 and #2 in pLentiCRISPR v2) were purchased from GenScript, and scrambled gRNA sequences were synthesized and then cloned into pLentiCRISPR v2. pDONR225-NF1 was a kind gift from the RAS Initiative at the Frederick National Laboratory for Cancer Research at NCI. The full-length *NF1* coding sequence in this vector has been extensively modified to facilitate expression studies without changing the amino acid sequence. To analyze its expression, an “*NF1 (NCI)*” primer set was used for RT-PCR. This *NF1* coding sequence is also refractory to both the C5 and C6 shRNA clones. *NF1* mutants were created by site-directed mutagenesis (QuickChange II XL Site-Directed Mutagenesis Kit, Agilent Technologies) using pDONR225-NF1 as the template. These cDNAs were finally transferred into destination vectors pCL-FLAG and pM (Chang et al., 1999) to create pCL-FLAG-NF1, pM-NF1, pCL-FLAG-NF1-R2258*, pCL-FLAG-NF1-Y2285*, pCL-FLAG-NF1-R2450*, pCL-FLAG-NF1-R1362Q, pM-NF1-R1362Q, pCL-FLAG-NF1-K1444R, pM-NF1-K1444R, pCL-FLAG-NF1-I417M, pM-NF1-I417M, pM-NF1-I417A/I418A, pCL-FLAG-NF1-V1308A/I1309A, and pM-NF1-V1308A/I1309A. pDEST566-NF1-M2/GAP (Bollag et al., 1993), which expresses recombinant 6×His-MBP tag at the N-terminus of NF1-M2/GAP in *E. coli*, was also a gift from the NCI RAS Initiative. pDEST566-GST was built by transferring GST cDNA from pENTR-GST to pDEST566.

Generation of *NF1* point mutation knock-in (KI) cells using CRISPR-Cas9

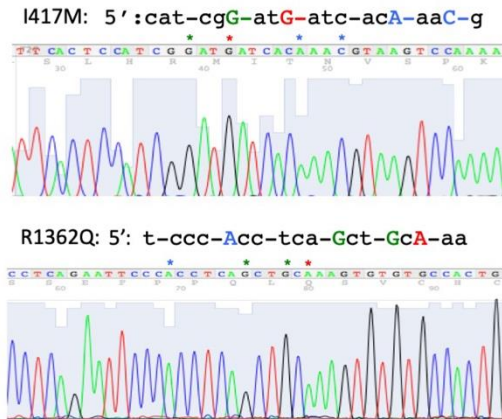
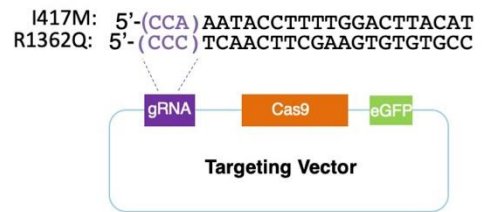
MCF-7 cells carrying homozygous mutations were generated by the Cell-Based Assay Screening Service core at Baylor College of Medicine (BCM). The general procedure is as described previously (Ran et al., 2013) and depicted in the right figure. Briefly, gRNA sequences were cloned into SpCas9(BB)-2A-GFP (PX458, a gift from Feng Zhang, Addgene plasmid #48138; <http://n2t.net/addgene:48138>;

RRID: Addgene_48138). In addition to silent mutations that prevent Cas9 cleavage, each single-stranded oligodeoxynucleotide

(ssODN) repair template also contains an engineered restriction site to facilitate identification of the KI allele. Cells were co-transfected with the CRISPR/gRNA plasmid and its corresponding ssODN template using the Neon transfection system (Thermo Fisher Scientific). The resulting GFP⁺ cells were plated by limiting dilution for single clone isolation. The genomic region surrounding each target site was PCR-amplified for sequencing to identify clones in which the wild-type allele was undetectable (Fig. 1 on the right).

Assays for cell growth and apoptosis

To compare cell growth between *NF1*⁺ and *NF1*^{KD} cells, cells stably expressing *NF1* shRNA were first seeded in estrogen-deprived medium, typically in triplicate, with DOX added at



(Color coding: red, targeting mutation; green, silent mutation for new BtsCI or PvuII site, and blue, silent mutations blocking Cas9 cleavage)

Knock-in design and confirmation by sequencing.

the same time. Two days later (Day-0), the medium was replaced with a fresh medium containing either vehicle control or compound(s) under investigation, with medium change every three days thereafter. The number of viable cells was measured using the CellTiter 96 Aqueous One Solution Cell Proliferation Assay kit (Promega) six days later (Day-6). Cell growth between parental and *NF1* knock-out cells was similarly examined except no DOX was added. Apoptosis was measured by FITC-Annexin (Becton Dickinson) staining followed by FACS.

Generation of NF1 antibodies

A cDNA encoding amino acid residues 2471-2839 in NF1 was subcloned into pRP259 (Chang et al., 1994) to express this C-terminal fragment of NF1 (NF1C) as a GST-tagged protein in *E. coli* (BL21 DE3). Purified GST-NF1C was injected into rabbits (Thermo Fisher Scientific) or mice (Protein and Monoclonal Antibody Production Shared Resource at BCM) to generate polyclonal and monoclonal antibodies, respectively. The polyclonal antibody from one rabbit (NF1 Ab-2, Figure S5A) was later affinity-purified against the same immunizing antigen. One hybridoma clone (mAb-376) was expanded *in vitro* and IgG was purified from culture medium by protein-G Sepharose column chromatography.

Immunoprecipitation (IP)

Cells grown in E2-deprived medium were treated with E2 (10^{-11} M), 4-OHT (10^{-7} M), or the vehicle (ethanol) for 4 hrs before being isolated for whole cell or nuclear extracts. To conduct IP using whole cell extracts, cells were lysed in RIPA buffer supplemented with 1 mM PMSF and protease and phosphatase inhibitors (Roche Applied Science). The cell lysates were pre-cleared with mouse IgG beads (Sigma, 3 hours at 4°C) before NF1 (mAb-376) or ER (F-10 monoclonal, Santa Cruz) antibody or the mouse IgG control (Santa Cruz) was added. Samples were incubated at 4°C overnight, followed by incubation with protein A/G agarose beads (Santa Cruz) for another

4 hours. All beads were finally washed three times with TBS (20 mM Tris-HCl (pH 7.5) and 150 mM NaCl). The bound proteins were eluted with 2× SDS sample buffer by boiling for 5 minutes and then examined by immunoblotting. To conduct IP using nuclear extracts, the same antibodies were pre-incubated with the protein-G Dynabeads™ (Thermo Fisher Scientific) overnight at 4°C before mixing with nuclear extracts which were prepared as described previously (Lanz et al., 2010). All beads were washed twice with NETN buffer (20 mM Tris-HCl (pH 7.5), 1 mM EDTA, 150 mM NaCl, and 0.5% NP-40), and once with PBS before elution and immunoblotting.

Immunoblotting

Cell lysates were generally prepared in RIPA buffer supplemented with protease and phosphatase inhibitors, and proteins were separated by SDS-PAGE before being transferred to nitrocellulose membranes. The primary antibodies used are listed in Key Resource Table. The fluorescein-conjugated secondary antibodies were from Li-COR Biosciences, and the protein levels were quantified by an Odyssey infrared imaging system (Li-COR Biosciences).

RNA-seq

Estrogen-deprived MCF-7 cells were treated with E2 (10^{-11} M), 4-OHT (10^{-7} M), or ethanol (vehicle) before RNA was extracted after 24 hrs using RNeasy Mini Kit (Qiagen) according to manufacturer's directions. The E2 concentration used in this and the ChIP experiment was chosen because it can efficiently differentiate the growth between NF1⁺ and NF1-depleted cells (Figure 1E). Because the E2 concentration used was low, pilot qPCR experiments were conducted to determine that it takes 24 hrs after E2 stimulation to observe substantial difference in gene expression between these cells. MCF-7 CRISPR KI cells were simply grown in estrogen deprivation medium for 72 hrs before RNA extraction. The Genomic and RNA Profiling Core

(GARP) at BCM constructed libraries with 250 ng of total RNA using the TruSeq RNA Library Prep Kit (Illumina). cDNA was generated from poly(A)-selected RNA. Libraries were quantified with the KAPA Library Quantification Kit (Kapa Biosystems) and were sequenced on the NextSeq 500 (Illumina) with paired-end 75bp reads and aligned to the hg19 (GRCh37) reference genome using RSEM v1.2.31 (Li and Dewey, 2011) and Bowtie 2 (Langmead and Salzberg, 2012).

Differential gene expression and fold change analysis was performed using EBseq (Leng et al., 2013) with FDR < 0.2 as a cutoff. Differentially expressed genes were subsequently used in Gene Set Enrichment Analysis (GSEA) for “Hallmark Pathways” in the Molecular Signatures Database (MSigDB) (Subramanian et al., 2005) and the top 10 enriched pathways were reported. For validation in clinical datasets, mRNA levels of the 1,107 genes identified from the MCF-7 cell line study were analyzed in TCGA and METABRIC ER⁺ breast cancer cohorts using cBioportal (Cerami et al., 2012; Gao et al., 2013). Genes in these cohorts that are differentially expressed between *NFI*-FS/NS and *NFI*-WT tumors were identified by t-test with p values cutoff at < 0.05. The differentially expressed genes in these clinical validation datasets were each similarly analyzed for “Hallmark” pathways enrichment as above (FDR<0.05). Clustering was performed using Hierarchical Clustering in R.

ChIP

The cells were seeded in E2-deprived medium. After 48 hrs, the cells were treated with E2 (10^{-11} M), 4-OHT (10^{-7} M), or the vehicle control (ethanol) for 45 min before ChIP, which was performed as described (Chen et al., 2008). Specifically, crosslinking was performed using 1% formaldehyde for 10 min at room temperature and quenched by glycine (final concentration of 125 mM). Cells were then scraped off the plate with ice-cold TBSE buffer (20 mM Tris-HCl, pH 7.5, 1.0 mM EDTA, 150 mM NaCl) and pelleted by centrifugation. Next, pelleted cells were

resuspended in lysis buffer (10 mM Tris-HCl, pH 8.0, 0.25% Triton X-100, 10 mM EDTA, 100 mM NaCl) to release nuclei. The nuclei were further lysed in 1% SDS buffer (50 mM HEPES-KOH, pH 7.5, 1% Triton X-100, 0.1% sodium deoxycholate, 1% SDS, 2 mM EDTA, 150 mM NaCl) and sonicated using a Branson Sonicator to shear genomic DNA to an average fragment size of 200 to 500 bp. ChIP was performed with a commercially available antibody against ER- α (HC-20 and F10 for ChIP-qPCR, and F10 for ChIP-seq, Santa Cruz), a rabbit polyclonal NF1 antibody (A300-140A from Bethyl Laboratories; Ab-1), a polyclonal NF1 antibody made by us (above; Ab-2), a rabbit IgG control (Millipore) or a mouse IgG control (Santa Cruz) added to the same amount of chromatin after SDS was diluted to 0.1%. The precipitated DNA was isolated by phenol-chloroform extraction. To assess ERE occupancy by qPCR, fold-enrichment of amplified ERE levels in the ChIPed samples vs. those in inputs were calculated.

qPCR

The general qPCR methods were as described (Zheng et al., 2015), and the primers employed are listed in Key Resource Table .

ERE-luciferase reporter assay

MCF-7 cells were seeded in E2-deprived medium for one day before being transfected with pGL2-ERE-Luc (Hall and McDonnell, 1999), which contains 3 \times vitellogenin EREs, for another day. The cells were then treated with 10⁻¹¹ M E2 for 24 hrs. Cells were also co-transfected with pGL4.70-RLuc (Promega, Madison, WI, USA) to express *Renilla* luciferase as an internal transfection efficiency control. The firefly and *Renilla* luciferase levels were measured using the Dual-Luciferase Reporter Assay kit (Promega).

The mammalian two-hybrid assay

The mammalian two-hybrid assays measuring the binding between ER and its coregulators have been described (Chang et al., 1999). Briefly, HEK293 cells were co-transfected by pM vectors expressing various versions of NF1 fused to the Gal4 DNA binding domain (DBD), as well as pVP16 vectors expressing various ER fragments fused to the VP16 transcriptional activation domain. These cells were also co-transfected to carry the firefly luciferase reporter 5×Gal4-Luc3 and the pGL4.70-RLuc, whose Renilla luciferase activity was measured to control transfection efficiency. Fusion protein expression levels were also assessed by Western blot. Luciferase activities were measured two days later. To determine whether the NF1-ER interaction can be modulated by E2 and 4-OHT, cells were estrogen-starved before transfection. E2 (10^{-11} M), 4-OHT (10^{-7} M), or the vehicle control was added one day post-transfection. The luciferase activity was measured after another day.

ER and NF1-M2/GAP *in vitro* binding assay

E. coli BL21 (DE3) cells carrying either pDEST566-GST or pDEST566-NF1-M2/GAP were induced by 1 mM IPTG at 30°C for 4 hrs. The cell pellets were then resuspended in ice-cold MBP binding buffer (20 mM Tris-HCl (pH 7.4), 200 mM NaCl, 1 mM EDTA, 1 mM DTT, 1 mM PMSF, and protease inhibitors) and sonicated. The cell lysates were incubated with amylose magnetic beads (New England Biolabs) for 4 hrs at 4°C and washed by the MBP binding buffer. After elution (2× SDS sample buffer), the concentrations of bound proteins on the beads were quantified using BSA as the standard. Purified recombinant ER- α (10 ng, Thermo Fisher Scientific) was pre-incubated with 100 nM E2, 5 μ M 4-OHT, or ethanol for 1 hr at 4°C, and then mixed with 200 ng bead-bound NF1-M2/GAP or the GST control, which was pre-incubated with 1 mg/ml BSA in MBP binding buffer for 1 hr at 4°C to reduce non-specific binding. After 1 hr at 4°C, the bound proteins were eluted with 2× SDS sample buffer and examined by immunoblotting.

Cell fractionation

The experiments were conducted as previously described (Suzuki et al., 2010). Leptomycin B (LMB) at 40 nM or ethanol (vehicle) was given to the cells grown in regular growth medium for 6 hours. To assess the influence of ER ligands, cells were first starved in E2-deprived medium and then treated with E2 (10^{-11} M), 4-OHT (10^{-7} M), or the vehicle control for 16 hours.

Immunofluorescence deconvolution microscopy

Cells were seeded and treated by LMB or ER-ligands (above) in 12-well plates with an 18-mm No. 1.5 coverslip. The fixation (4% formaldehyde), permeabilization (200 mM glycine/1X PBS, 0.1% Triton X-100), and blocking (5% goat serum) were performed as previously described (Cheng et al., 2011). The sample was incubated with NF1 antibody mAb-376 at room temperature for 2.5 hrs. We found that it is important to optimize the dilution factor for the secondary antibody to reduce background. Alexa-Fluor™ 488 conjugated goat anti-mouse IgG secondary Ab (Thermo Fisher Scientific) was added after a 1:1,000 dilution in the blocking solution and incubation was performed in the dark for 1 hr. The samples were then mounted to slides with a DAPI-containing mounting medium (Vector Laboratories). Imaging was performed at the Integrated Microscopy Core at BCM on a DVLive epifluorescence image restoration microscope (GE Healthcare). The system is equipped with an Olympus PlanApo 60×/1.42 N.A. objective and a pco.EDGE sCMOS_5.5 camera with a resolution up to 2,560 × 2,160 pixels. The filter sets used were: DAPI and FITC. Z stacks (0.2 μm) covering the whole cell (~12 μm) were acquired before applying a conservative restorative algorithm for quantitative image deconvolution using SoftWorx v7.0. Image J was used to quantify NF1 levels. For each cell a single focal plane dissecting the middle of the nucleus was chosen, from which two ROIs were created: ROI-1 encircles the whole cell

while ROI-2 encircles just the nucleus. The reported relative NF1 nuclear levels were defined as: ROI-2/ROI-1.

ERE pull-down using HeLa cell nuclear extract

These assays were conducted similarly to those previously described (Foulds et al., 2013). Briefly, 1 mg of HeLa S3 nuclear extract and 0.5 µg of purified recombinant ER were added to 4 µg of a 921 bp biotinylated 4× ERE DNA fragment immobilized onto 60 µl Dynabeads™ M280 (Thermo Fisher Scientific). Different ligands were included in these recruitment assays. After washing twice in NETN and once in DPBS, the retained proteins were detected by immunoblotting.

QUANTIFICATION AND STATISTICAL ANALYSIS

All reported data were typically presented as mean ± s.e.m. and pair-wise comparisons were analyzed by two-sided Student's t-test unless otherwise mentioned. The n values are either separate biological replicates or numbers of cells or mice, as indicated. Human tumor databases were analyzed using the R statistical packages. We note that throughout this paper *, p<0.05; **, p<0.01; ***, p<0.001; NS, Not Significant (p≥0.05).

***NF1* mutation frequency in patients**

The extraction and general sequencing pipeline of cell-free DNA has been described previously (Lanman et al., 2015). Specifically, for *NF1*, most of its exons (except exons 1, 7, 15, 19, 22, 23, 29, 31, 51, and 56-61) were completely sequenced, and single nucleotide variants as well as small indel events were analyzed. M1 and M2 are encoded by exons 11 (25 amino acids) and 29 (35 amino acids). cBio (Cerami et al., 2012) was used for somatic mutation and clinical data mining. Mutations were visualized using the GeneVisR (Skidmore et al., 2016) Bioconductor

package. The cohort of primary breast cancers was from TCGA (TCGA, 2012), while the metastatic cohort was described (Lanman et al., 2015).

Patient proliferation status after aromatase inhibitor (AI) treatments

Patients in the ACOSOG Z1031 trial (Ellis et al., 2011) were treated by AIs in a neoadjuvant setting, and their mRNAs before and after treatment were analyzed by Agilent microarray. A multigene proliferation score (MGPS) derived from mRNA expression of 772 genes was used to analyze proliferation status in the patient to assess treatment response (Ellis et al., 2017).

***NFI* expression level analysis in patients**

NFI mutation types in TCGA (Ciriello et al., 2015) and METABRIC (Pereira et al., 2016) were mined from cBio (Cerami et al., 2012; Gao et al., 2013). *NFI* mRNA levels in ER⁺ breast tumors from the METABRIC cohort (Curtis et al., 2012) together with survival information were obtained from Oncomine (Rhodes et al., 2007). High and low *NFI* mRNA levels were as defined above. Univariate Cox regression was analyzed using the Survival package for R.

Protein levels correlation analysis

We have previously shown that protein co-expression is a strong predictor for co-functionality (Wang et al., 2017a). To identify proteins co-expressed with NF1, we used the LinkedOmics tool (<http://www.linkedomics.org>) (Vasaikar et al., 2018) to calculate the Pearson's correlation coefficient between NF1 and all other proteins in the CPTAC (Clinical Proteomic Tumor Analysis Consortium) breast cancer mass spectrometry dataset, which contains 105 breast tumor samples (Mertins et al., 2016). We ranked the proteins based on correlation coefficient scores and then analyzed them using Gene Set Enrichment Analysis (GSEA) in WebGestalt (Wang

et al., 2017b) to identify enriched Gene Ontology (GO) molecular functions. As a control, we similarly analyzed p120GAP/RASA1.

DATA AND SOFTWARE AVAILABILITY

The datasets in this study are available in NIH Gene Expression Omnibus with the accession numbers listed in Key Resource Table.

References

- Anbalagan, M., and Rowan, B. G. (2015). Estrogen receptor alpha phosphorylation and its functional impact in human breast cancer. *Mol Cell Endocrinol* *418 Pt 3*, 264-272.
- Ballester, R., Marchuk, D., Boguski, M., Saulino, A., Letcher, R., Wigler, M., and Collins, F. (1990). The NF1 locus encodes a protein functionally related to mammalian GAP and yeast IRA proteins. *Cell* *63*, 851-859.
- Beausoleil, S. A., Jedrychowski, M., Schwartz, D., Elias, J. E., Villen, J., Li, J., Cohn, M. A., Cantley, L. C., and Gygi, S. P. (2004). Large-scale characterization of HeLa cell nuclear phosphoproteins. *Proc Natl Acad Sci U S A* *101*, 12130-12135.
- Berto, M., Jean, V., Zwart, W., and Picard, D. (2018). ERalpha activity depends on interaction and target site corecruitment with phosphorylated CREB1. *Life Sci Alliance* *1*, e201800055.
- Bertucci, F., Ng, C. K. Y., Patsouris, A., Droin, N., Piscuoglio, S., Carbuccia, N., Soria, J. C., Dien, A. T., Adnani, Y., Kamal, M., *et al.* (2019). Genomic characterization of metastatic breast cancers. *Nature* *569*, 560-564.
- Bollag, G., McCormick, F., and Clark, R. (1993). Characterization of full-length neurofibromin: tubulin inhibits Ras GAP activity. *EMBO J* *12*, 1923-1927.
- Borromeo, M. D., Savage, T. K., Kollipara, R. K., He, M., Augustyn, A., Osborne, J. K., Girard, L., Minna, J. D., Gazdar, A. F., Cobb, M. H., and Johnson, J. E. (2016). ASCL1 and NEUROD1 Reveal Heterogeneity in Pulmonary Neuroendocrine Tumors and Regulate Distinct Genetic Programs. *Cell Rep* *16*, 1259-1272.
- Carroll, J. S., Liu, X. S., Brodsky, A. S., Li, W., Meyer, C. A., Szary, A. J., Eeckhoute, J., Shao, W., Hestermann, E. V., Geistlinger, T. R., *et al.* (2005). Chromosome-wide mapping of estrogen receptor binding reveals long-range regulation requiring the forkhead protein FoxA1. *Cell* *122*, 33-43.
- Carroll, J. S., Meyer, C. A., Song, J., Li, W., Geistlinger, T. R., Eeckhoute, J., Brodsky, A. S., Keeton, E. K., Fertuck, K. C., Hall, G. F., *et al.* (2006). Genome-wide analysis of estrogen receptor binding sites. *Nat Genet* *38*, 1289-1297.
- Cerami, E., Gao, J., Dogrusoz, U., Gross, B. E., Sumer, S. O., Aksoy, B. A., Jacobsen, A., Byrne, C. J., Heuer, M. L., Larsson, E., *et al.* (2012). The cBio cancer genomics portal: an open platform for exploring multidimensional cancer genomics data. *Cancer discovery* *2*, 401-404.
- Chang, C., Norris, J. D., Gron, H., Paige, L. A., Hamilton, P. T., Kenan, D. J., Fowlkes, D., and McDonnell, D. P. (1999). Dissection of the LXXLL nuclear receptor-coactivator interaction motif using combinatorial peptide libraries: discovery of peptide antagonists of estrogen receptors alpha and beta. *Mol Cell Biol* *19*, 8226-8239.
- Chang, E. C., Barr, M., Wang, Y., Jung, V., Xu, H., and Wigler, H. M. (1994). Cooperative interaction of *S. pombe* proteins required for mating and morphogenesis. *Cell* *79*, 131-141.
- Chen, X., Xu, H., Yuan, P., Fang, F., Huss, M., Vega, V. B., Wong, E., Orlov, Y. L., Zhang, W., Jiang, J., *et al.* (2008). Integration of external signaling pathways with the core transcriptional network in embryonic stem cells. *Cell* *133*, 1106-1117.
- Cheng, C. M., Li, H., Gasman, S., Huang, J., Schiff, R., and Chang, E. C. (2011). Compartmentalized Ras proteins transform NIH 3T3 cells with different efficiencies. *Mol Cell Biol* *31*, 983-997.

Ciriello, G., Gatz, M. L., Beck, A. H., Wilkerson, M. D., Rhie, S. K., Pastore, A., Zhang, H., McLellan, M., Yau, C., Kandoth, C., *et al.* (2015). Comprehensive Molecular Portraits of Invasive Lobular Breast Cancer. *Cell* 163, 506-519.

Curtis, C., Shah, S. P., Chin, S. F., Turashvili, G., Rueda, O. M., Dunning, M. J., Speed, D., Lynch, A. G., Samarajiwa, S., Yuan, Y., *et al.* (2012). The genomic and transcriptomic architecture of 2,000 breast tumours reveals novel subgroups. *Nature* 486, 346-352.

Daston, M. M., Scrable, H., Nordlund, M., Sturbaum, A. K., Nissen, L. M., and Ratner, N. (1992). The protein product of the neurofibromatosis type 1 gene is expressed at highest abundance in neurons, Schwann cells, and oligodendrocytes. *Neuron* 8, 415-428.

de Cremoux, P., Bieche, I., Tran-Perennou, C., Vignaud, S., Boudou, E., Asselain, B., Lidereau, R., Magdelenat, H., Becette, V., Sigal-Zafrani, B., and Spyrtatos, F. (2004). Inter-laboratory quality control for hormone-dependent gene expression in human breast tumors using real-time reverse transcription-polymerase chain reaction. *Endocr Relat Cancer* 11, 489-495.

Diggs-Andrews, K. A., Brown, J. A., Gianino, S. M., Rubin, J. B., Wozniak, D. F., and Gutmann, D. H. (2014). Sex Is a major determinant of neuronal dysfunction in neurofibromatosis type 1. *Ann Neurol* 75, 309-316.

Ding, Y., Li, N., Dong, B., Guo, W., Wei, H., Chen, Q., Yuan, H., Han, Y., Chang, H., Kan, S., *et al.* (2019). Chromatin remodeling ATPase BRG1 and PTEN are synthetic lethal in prostate cancer. *J Clin Invest* 129, 759-773.

Dischinger, P. S., Tovar, E. A., Essenburg, C. J., Madaj, Z. B., Gardner, E. E., Callaghan, M. E., Turner, A. N., Challa, A. K., Kempston, T., Eagleson, B., *et al.* (2018). NF1 deficiency correlates with estrogen receptor signaling and diminished survival in breast cancer. *NPJ Breast Cancer* 4, 29.

Dombi, E., Baldwin, A., Marcus, L. J., Fisher, M. J., Weiss, B., Kim, A., Whitcomb, P., Martin, S., Aschbacher-Smith, L. E., Rizvi, T. A., *et al.* (2016). Activity of Selumetinib in Neurofibromatosis Type 1-Related Plexiform Neurofibromas. *N Engl J Med* 375, 2550-2560.

Ellis, M. J., Gao, F., Dehdashti, F., Jeffe, D. B., Marcom, P. K., Carey, L. A., Dickler, M. N., Silverman, P., Fleming, G. F., Kommareddy, A., *et al.* (2009). Lower-dose vs high-dose oral estradiol therapy of hormone receptor-positive, aromatase inhibitor-resistant advanced breast cancer: a phase 2 randomized study. *JAMA* 302, 774-780.

Ellis, M. J., Suman, V. J., Hoog, J., Goncalves, R., Sanati, S., Creighton, C. J., DeSchryver, K., Crouch, E., Brink, A., Watson, M., *et al.* (2017). Ki67 Proliferation Index as a Tool for Chemotherapy Decisions During and After Neoadjuvant Aromatase Inhibitor Treatment of Breast Cancer: Results From the American College of Surgeons Oncology Group Z1031 Trial (Alliance). *J Clin Oncol* 35, 1061-1069.

Ellis, M. J., Suman, V. J., Hoog, J., Lin, L., Snider, J., Prat, A., Parker, J. S., Luo, J., DeSchryver, K., Allred, D. C., *et al.* (2011). Randomized phase II neoadjuvant comparison between letrozole, anastrozole, and exemestane for postmenopausal women with estrogen receptor-rich stage 2 to 3 breast cancer: clinical and biomarker outcomes and predictive value of the baseline PAM50-based intrinsic subtype--ACOSOG Z1031. *J Clin Oncol* 29, 2342-2349.

Feng, Q., and O'Malley, B. W. (2014). Nuclear receptor modulation--role of coregulators in selective estrogen receptor modulator (SERM) actions. *Steroids* 90, 39-43.

Foulds, C. E., Feng, Q., Ding, C., Bailey, S., Hunsaker, T. L., Malovannaya, A., Hamilton, R. A., Gates, L. A., Zhang, Z., Li, C., *et al.* (2013). Proteomic analysis of coregulators bound to ERalpha on DNA and nucleosomes reveals coregulator dynamics. *Mol Cell* 51, 185-199.

Gao, J., Aksoy, B. A., Dogrusoz, U., Dresdner, G., Gross, B., Sumer, S. O., Sun, Y., Jacobsen, A., Sinha, R., Larsson, E., *et al.* (2013). Integrative analysis of complex cancer genomics and clinical profiles using the cBioPortal. *Sci Signal* 6, p11.

Gates, L. A., Gu, G., Chen, Y., Rohira, A. D., Lei, J. T., Hamilton, R. A., Yu, Y., Lonard, D. M., Wang, J., Wang, S. P., *et al.* (2018). Proteomic profiling identifies key coactivators utilized by mutant ERalpha proteins as potential new therapeutic targets. *Oncogene* 37, 4581-4598.

Glont, S. E., Chernukhin, I., and Carroll, J. S. (2019). Comprehensive Genomic Analysis Reveals that the Pioneering Function of FOXA1 Is Independent of Hormonal Signaling. *Cell Rep* 26, 2558-2565 e2553.

Griffith, O. L., Spies, N. C., Anurag, M., Griffith, M., Luo, J., Tu, D., Yeo, B., Kunisaki, J., Miller, C. A., Krysiak, K., *et al.* (2018). The prognostic effects of somatic mutations in ER-positive breast cancer. *Nature communications* 9, 3476.

Grisouard, J., Medunjanin, S., Hermani, A., Shukla, A., and Mayer, D. (2007). Glycogen synthase kinase-3 protects estrogen receptor alpha from proteasomal degradation and is required for full transcriptional activity of the receptor. *Mol Endocrinol* 21, 2427-2439.

Gross, A. M., Wolters, P., Baldwin, A., Dombi, E., Fisher, M. J., Weiss, B. D., AeRang Kim, Blakeley, J. O. N., Whitcomb, P., Holmblad, M., *et al.* (2018). SPRINT: Phase II study of the MEK 1/2 inhibitor selumetinib (AZD6244, ARRY-142886) in children with neurofibromatosis type 1 (NF1) and inoperable plexiform neurofibromas (PN). *J Clin Onco* 36, 10503-10503.

Hall, J. M., and McDonnell, D. P. (1999). The estrogen receptor beta-isoform (ERbeta) of the human estrogen receptor modulates ERalpha transcriptional activity and is a key regulator of the cellular response to estrogens and antiestrogens. *Endocrinology* 140, 5566-5578.

Harrod, A., Fulton, J., Nguyen, V. T. M., Periyasamy, M., Ramos-Garcia, L., Lai, C. F., Metodieva, G., de Giorgio, A., Williams, R. L., Santos, D. B., *et al.* (2017). Genomic modelling of the ESR1 Y537S mutation for evaluating function and new therapeutic approaches for metastatic breast cancer. *Oncogene* 36, 2286-2296.

He, H., Sinha, I., Fan, R., Haldosen, L. A., Yan, F., Zhao, C., and Dahlman-Wright, K. (2018). c-Jun/AP-1 overexpression reprograms ERalpha signaling related to tamoxifen response in ERalpha-positive breast cancer. *Oncogene* 37, 2586-2600.

Heinz, S., Benner, C., Spann, N., Bertolino, E., Lin, Y. C., Laslo, P., Cheng, J. X., Murre, C., Singh, H., and Glass, C. K. (2010). Simple combinations of lineage-determining transcription factors prime cis-regulatory elements required for macrophage and B cell identities. *Mol Cell* 38, 576-589.

Heldring, N., Pawson, T., McDonnell, D., Treuter, E., Gustafsson, J. A., and Pike, A. C. (2007). Structural insights into corepressor recognition by antagonist-bound estrogen receptors. *J Biol Chem* 282, 10449-10455.

Hu, X., and Lazar, M. A. (1999). The CoRNR motif controls the recruitment of corepressors by nuclear hormone receptors. *Nature* 402, 93-96.

Huang, H. J., Norris, J. D., and McDonnell, D. P. (2002). Identification of a negative regulatory surface within estrogen receptor alpha provides evidence in support of a role for corepressors in regulating cellular responses to agonists and antagonists. *Mol Endocrinol* 16, 1778-1792.

Huang, K. L., Li, S., Mertins, P., Cao, S., Gunawardena, H. P., Ruggles, K. V., Mani, D. R., Clauser, K. R., Tanioka, M., Usary, J., *et al.* (2017). Proteogenomic integration reveals therapeutic targets in breast cancer xenografts. *Nature communications* 8, 14864.

Jeselson, R., Bergholz, J. S., Pun, M., Cornwell, M., Liu, W., Nardone, A., Xiao, T., Li, W., Qiu, X., Buchwalter, G., *et al.* (2018). Allele-Specific Chromatin Recruitment and Therapeutic Vulnerabilities of ESR1 Activating Mutations. *Cancer Cell* 33, 173-186 e175.

Karmakar, S., Jin, Y., and Nagaich, A. K. (2013). Interaction of glucocorticoid receptor (GR) with estrogen receptor (ER) alpha and activator protein 1 (AP1) in dexamethasone-mediated interference of ERalpha activity. *J Biol Chem* 288, 24020-24034.

Kato, S., Endoh, H., Masuhiro, Y., Kitamoto, T., Uchiyama, S., Sasaki, H., Masushige, S., Gotoh, Y., Nishida, E., Kawashima, H., *et al.* (1995). Activation of the estrogen receptor through phosphorylation by mitogen-activated protein kinase. *Science* 270, 1491-1494.

Kininis, M., Isaacs, G. D., Core, L. J., Hah, N., and Kraus, W. L. (2009). Postrecruitment regulation of RNA polymerase II directs rapid signaling responses at the promoters of estrogen target genes. *Mol Cell Biol* 29, 1123-1133.

Koliou, X., Fedonidis, C., Kalpachidou, T., and Mangoura, D. (2016). Nuclear import mechanism of neurofibromin for localization on the spindle and function in chromosome congression. *J Neurochem* 136, 78-91.

Kweh, F., Zheng, M., Kurenova, E., Wallace, M., Golubovskaya, V., and Cance, W. G. (2009). Neurofibromin physically interacts with the N-terminal domain of focal adhesion kinase. *Mol Carcinog* 48, 1005-1017.

Langmead, B., and Salzberg, S. L. (2012). Fast gapped-read alignment with Bowtie 2. *Nat Methods* 9, 357-359.

Lanman, R. B., Mortimer, S. A., Zill, O. A., Sebisano, D., Lopez, R., Blau, S., Collisson, E. A., Divers, S. G., Hoon, D. S., Kopetz, E. S., *et al.* (2015). Analytical and Clinical Validation of a Digital Sequencing Panel for Quantitative, Highly Accurate Evaluation of Cell-Free Circulating Tumor DNA. *PLoS One* 10, e0140712.

Lanz, R. B., Bulynko, Y., Malovannaya, A., Labhart, P., Wang, L., Li, W., Qin, J., Harper, M., and O'Malley, B. W. (2010). Global characterization of transcriptional impact of the SRC-3 coregulator. *Mol Endocrinol* 24, 859-872.

Lei, J. T., Shao, J., Zhang, J., Iglesia, M., Chan, D. W., Cao, J., Anurag, M., Singh, P., He, X., Kosaka, Y., *et al.* (2018). Functional Annotation of ESR1 Gene Fusions in Estrogen Receptor-Positive Breast Cancer. *Cell reports* 24, 1434-1444 e1437.

Leng, N., Dawson, J. A., Thomson, J. A., Ruotti, V., Rissman, A. I., Smits, B. M., Haag, J. D., Gould, M. N., Stewart, R. M., and Kendzioriski, C. (2013). EBSeq: an empirical Bayes hierarchical model for inference in RNA-seq experiments. *Bioinformatics* 29, 1035-1043.

Li, B., and Dewey, C. N. (2011). RSEM: accurate transcript quantification from RNA-Seq data with or without a reference genome. *BMC Bioinformatics* 12, 323.

Li, C., Cheng, Y., Gutmann, D. A., and Mangoura, D. (2001). Differential localization of the neurofibromatosis 1 (NF1) gene product, neurofibromin, with the F-actin or microtubule cytoskeleton during differentiation of telencephalic neurons. *Brain Res Dev Brain Res* 130, 231-248.

Li, S., Shen, D., Shao, J., Crowder, R., Liu, W., Prat, A., He, X., Liu, S., Hoog, J., Lu, C., *et al.* (2013). Endocrine-therapy-resistant ESR1 variants revealed by genomic characterization of breast-cancer-derived xenografts. *Cell reports* 4, 1116-1130.

Lin, C. Y., Strom, A., Vega, V. B., Kong, S. L., Yeo, A. L., Thomsen, J. S., Chan, W. C., Doray, B., Bangarusamy, D. K., Ramasamy, A., *et al.* (2004). Discovery of estrogen receptor alpha target genes and response elements in breast tumor cells. *Genome Biol* 5, R66.

Lonard, D. M., Nawaz, Z., Smith, C. L., and O'Malley, B. W. (2000). The 26S proteasome is required for estrogen receptor-alpha and coactivator turnover and for efficient estrogen receptor-alpha transactivation. *Mol Cell* 5, 939-948.

Madanikia, S. A., Bergner, A., Ye, X., and Blakeley, J. O. (2012). Increased risk of breast cancer in women with NF1. *American journal of medical genetics Part A* 158A, 3056-3060.

Maertens, O., and Cichowski, K. (2014). An expanding role for RAS GTPase activating proteins (RAS GAPs) in cancer. *Adv Biol Regul* 55, 1-14.

Martin, L. A., Ribas, R., Simigdala, N., Schuster, E., Pancholi, S., Tenev, T., Gellert, P., Buluwela, L., Harrod, A., Thornhill, A., *et al.* (2017). Discovery of naturally occurring ESR1 mutations in breast cancer cell lines modelling endocrine resistance. *Nature communications* 8, 1865.

Meric-Bernstam, F., Frampton, G. M., Ferrer-Lozano, J., Yelensky, R., Perez-Fidalgo, J. A., Wang, Y., Palmer, G. A., Ross, J. S., Miller, V. A., Su, X., *et al.* (2014). Concordance of genomic alterations between primary and recurrent breast cancer. *Mol Cancer Ther* 13, 1382-1389.

Mertins, P., Mani, D. R., Ruggles, K. V., Gillette, M. A., Clauser, K. R., Wang, P., Wang, X., Qiao, J. W., Cao, S., Petralia, F., *et al.* (2016). Proteogenomics connects somatic mutations to signalling in breast cancer. *Nature* 534, 55-62.

Nawaz, Z., Lonard, D. M., Dennis, A. P., Smith, C. L., and O'Malley, B. W. (1999). Proteasome-dependent degradation of the human estrogen receptor. *Proc Natl Acad Sci U S A* 96, 1858-1862.

Neve, R. M., Chin, K., Fridlyand, J., Yeh, J., Baehner, F. L., Fevr, T., Clark, L., Bayani, N., Coppe, J. P., Tong, F., *et al.* (2006). A collection of breast cancer cell lines for the study of functionally distinct cancer subtypes. *Cancer Cell* 10, 515-527.

Nik-Zainal, S., Davies, H., Staaf, J., Ramakrishna, M., Glodzik, D., Zou, X., Martincorena, I., Alexandrov, L. B., Martin, S., Wedge, D. C., *et al.* (2016). Landscape of somatic mutations in 560 breast cancer whole-genome sequences. *Nature*.

Nousiainen, M., Sillje, H. H., Sauer, G., Nigg, E. A., and Korner, R. (2006). Phosphoproteome analysis of the human mitotic spindle. *Proc Natl Acad Sci U S A* 103, 5391-5396.

Ogata, H., Sato, H., Takatsuka, J., and De Luca, L. M. (2001). Human breast cancer MDA-MB-231 cells fail to express the neurofibromin protein, lack its type I mRNA isoform and show accumulation of P-MAPK and activated Ras. *Cancer Lett* 172, 159-164.

Paschou, M., and Doxakis, E. (2012). Neurofibromin 1 is a miRNA target in neurons. *PLoS One* 7, e46773.

Pearson, A., Proszek, P. Z., Pascual, J., Fribbens, C., Shamsher, M. K., Kingston, B., O'Leary, B., Herrera-Abreu, M. T., Cutts, R. J., Garcia-Murillas, I., *et al.* (2019). Inactivating NF1 mutations are enriched in advanced breast cancer and contribute to endocrine therapy resistance. *Clin Cancer Res*.

Pereira, B., Chin, S. F., Rueda, O. M., Vollan, H. K., Provenzano, E., Bardwell, H. A., Pugh, M., Jones, L., Russell, R., Sammut, S. J., *et al.* (2016). The somatic mutation profiles of 2,433 breast cancers refines their genomic and transcriptomic landscapes. *Nature communications* 7, 11479.

Ramirez, F., Ryan, D. P., Gruning, B., Bhardwaj, V., Kilpert, F., Richter, A. S., Heyne, S., Dunder, F., and Manke, T. (2016). deepTools2: a next generation web server for deep-sequencing data analysis. *Nucleic Acids Res* 44, W160-165.

Ran, F. A., Hsu, P. D., Wright, J., Agarwala, V., Scott, D. A., and Zhang, F. (2013). Genome engineering using the CRISPR-Cas9 system. *Nat Protoc* 8, 2281-2308.

Ratner, N., and Miller, S. J. (2015). A RASopathy gene commonly mutated in cancer: the neurofibromatosis type 1 tumour suppressor. *Nat Rev Cancer* *15*, 290-301.

Razavi, P., Chang, M. T., Xu, G., Bandlamudi, C., Ross, D. S., Vasani, N., Cai, Y., Bielski, C. M., Donoghue, M. T. A., Jonsson, P., *et al.* (2018). The Genomic Landscape of Endocrine-Resistant Advanced Breast Cancers. *Cancer Cell* *34*, 427-438 e426.

Reid, G., Hubner, M. R., Metivier, R., Brand, H., Denger, S., Manu, D., Beaudouin, J., Ellenberg, J., and Gannon, F. (2003). Cyclic, proteasome-mediated turnover of unliganded and liganded ERalpha on responsive promoters is an integral feature of estrogen signaling. *Mol Cell* *11*, 695-707.

Rhodes, D. R., Kalyana-Sundaram, S., Mahavisno, V., Varambally, R., Yu, J., Briggs, B. B., Barrette, T. R., Anstet, M. J., Kincead-Beal, C., Kulkarni, P., *et al.* (2007). OncoPrint 3.0: genes, pathways, and networks in a collection of 18,000 cancer gene expression profiles. *Neoplasia* *9*, 166-180.

Robert, C., Karaszewska, B., Schachter, J., Rutkowski, P., Mackiewicz, A., Stroiakovski, D., Lichinitser, M., Dummer, R., Grange, F., Mortier, L., *et al.* (2015). Improved overall survival in melanoma with combined dabrafenib and trametinib. *N Engl J Med* *372*, 30-39.

Robinson, S. P., and Jordan, V. C. (1989). Antiestrogenic action of toremifene on hormone-dependent, -independent, and heterogeneous breast tumor growth in the athymic mouse. *Cancer Res* *49*, 1758-1762.

Rogers, S. A., Llewellyn, L., Wigham, T., and Sweeney, G. E. (2000). Cloning of the Atlantic salmon (*Salmo salar*) estrogen receptor-alpha gene. *Comp Biochem Physiol B Biochem Mol Biol* *125*, 379-385.

Salemis, N. S., Nakos, G., Sambaziotis, D., and Gourgiotis, S. (2010). Breast cancer associated with type 1 neurofibromatosis. *Breast Cancer* *17*, 306-309.

Schneider, C. A., Rasband, W. S., and Eliceiri, K. W. (2012). NIH Image to ImageJ: 25 years of image analysis. *Nat Methods* *9*, 671-675.

Shang, Y., Hu, X., DiRenzo, J., Lazar, M. A., and Brown, M. (2000). Cofactor dynamics and sufficiency in estrogen receptor-regulated transcription. *Cell* *103*, 843-852.

Sharif, S., Moran, A., Huson, S. M., Iddenden, R., Shenton, A., Howard, E., and Evans, D. G. (2007). Women with neurofibromatosis 1 are at a moderately increased risk of developing breast cancer and should be considered for early screening. *Journal of Medical Genetics* *44*, 481-484.

Shiau, A. K., Barstad, D., Loria, P. M., Cheng, L., Kushner, P. J., Agard, D. A., and Greene, G. L. (1998). The structural basis of estrogen receptor/coactivator recognition and the antagonism of this interaction by tamoxifen. *Cell* *95*, 927-937.

Skidmore, Z. L., Wagner, A. H., Lesurf, R., Campbell, K. M., Kunisaki, J., Griffith, O. L., and Griffith, M. (2016). GenVisR: Genomic Visualizations in R. *Bioinformatics* *32*, 3012-3014.

Sokol, E. S., Feng, Y. X., Jin, D. X., Basudan, A., Lee, A. V., Atkinson, J. M., Chen, J., Stephens, P. J., Frampton, G. M., Gupta, P. B., *et al.* (2019). Loss of function of NF1 is a mechanism of acquired resistance to endocrine therapy in lobular breast cancer. *Ann Oncol* *30*, 115-123.

Subramanian, A., Tamayo, P., Mootha, V. K., Mukherjee, S., Ebert, B. L., Gillette, M. A., Paulovich, A., Pomeroy, S. L., Golub, T. R., Lander, E. S., and Mesirov, J. P. (2005). Gene set enrichment analysis: a knowledge-based approach for interpreting genome-wide expression profiles. *Proc Natl Acad Sci U S A* *102*, 15545-15550.

Suzuki, K., Bose, P., Leong-Quong, R. Y., Fujita, D. J., and Riabowol, K. (2010). REAP: A two minute cell fractionation method. *BMC Res Notes* *3*, 294.

TCGA (2012). Comprehensive molecular portraits of human breast tumours. *Nature* 490, 61-70.

Trojaniello, C., Festino, L., Vanella, V., and Ascierto, P. A. (2019). Encorafenib in combination with binimetinib for unresectable or metastatic melanoma with BRAF mutations. *Expert Rev Clin Pharmacol* 12, 259-266.

Vandenbroucke, I., Van Oostveldt, P., Coene, E., De Paepe, A., and Messiaen, L. (2004). Neurofibromin is actively transported to the nucleus. *FEBS Lett* 560, 98-102.

Vasaikar, S. V., Straub, P., Wang, J., and Zhang, B. (2018). LinkedOmics: analyzing multi-omics data within and across 32 cancer types. *Nucleic Acids Res* 46, D956-D963.

Wang, H., Liu, C., Liu, X., Wang, M., Wu, D., Gao, J., Su, P., Nakahata, T., Zhou, W., Xu, Y., *et al.* (2018). MEIS1 Regulates Hemogenic Endothelial Generation, Megakaryopoiesis, and Thrombopoiesis in Human Pluripotent Stem Cells by Targeting TAL1 and FLI1. *Stem Cell Reports* 10, 447-460.

Wang, J., Ma, Z., Carr, S. A., Mertins, P., Zhang, H., Zhang, Z., Chan, D. W., Ellis, M. J., Townsend, R. R., Smith, R. D., *et al.* (2017a). Proteome Profiling Outperforms Transcriptome Profiling for Coexpression Based Gene Function Prediction. *Mol Cell Proteomics* 16, 121-134.

Wang, J., Vasaikar, S., Shi, Z., Greer, M., and Zhang, B. (2017b). WebGestalt 2017: a more comprehensive, powerful, flexible and interactive gene set enrichment analysis toolkit. *Nucleic Acids Res* 45, W130-W137.

Wang, Y., Lonard, D. M., Yu, Y., Chow, D. C., Palzkill, T. G., Wang, J., Qi, R., Matzuk, A. J., Song, X., Madoux, F., *et al.* (2014). Bufalin is a potent small-molecule inhibitor of the steroid receptor coactivators SRC-3 and SRC-1. *Cancer Res* 74, 1506-1517.

Wilkins, A. D., Bachman, B. J., Erdin, S., and Lichtarge, O. (2012). The use of evolutionary patterns in protein annotation. *Current Opinion in Structural Biology* 22, 316-325.

Won Jeong, K., Chodankar, R., Purcell, D. J., Bittencourt, D., and Stallcup, M. R. (2012). Gene-specific patterns of coregulator requirements by estrogen receptor-alpha in breast cancer cells. *Mol Endocrinol* 26, 955-966.

Yap, Y. S., McPherson, J. R., Ong, C. K., Rozen, S. G., Teh, B. T., Lee, A. S., and Callen, D. F. (2014). The NF1 gene revisited - from bench to bedside. *Oncotarget* 5, 5873-5892.

Yates, L. R., Knappskog, S., Wedge, D., Farmery, J. H. R., Gonzalez, S., Martincorena, I., Alexandrov, L. B., Van Loo, P., Haugland, H. K., Lilleng, P. K., *et al.* (2017). Genomic Evolution of Breast Cancer Metastasis and Relapse. *Cancer Cell* 32, 169-184 e167.

Zaman, K., Winterhalder, R., Mamot, C., Hasler-Strub, U., Rochlitz, C., Mueller, A., Berset, C., Wilidors, H., Perey, L., Rudolf, C. B., *et al.* (2015). Fulvestrant with or without selumetinib, a MEK 1/2 inhibitor, in breast cancer progressing after aromatase inhibitor therapy: a multicentre randomised placebo-controlled double-blind phase II trial, SAKK 21/08. *Eur J Cancer* 51, 1212-1220.

Zhang, Y., Liu, T., Meyer, C. A., Eeckhoute, J., Johnson, D. S., Bernstein, B. E., Nusbaum, C., Myers, R. M., Brown, M., Li, W., and Liu, X. S. (2008). Model-based analysis of ChIP-Seq (MACS). *Genome Biol* 9, R137.

Zheng, Z. Y., Bay, B. H., Aw, S. E., and Lin, V. C. (2005). A novel antiestrogenic mechanism in progesterone receptor-transfected breast cancer cells. *J Biol Chem* 280, 17480-17487.

Zheng, Z. Y., Cheng, C. M., Fu, X. R., Chen, L. Y., Xu, L., Terrillon, S., Wong, S. T., Bar-Sagi, D., Songyang, Z., and Chang, E. C. (2012). CHMP6 and VPS4A mediate the recycling of Ras to the plasma membrane to promote growth factor signaling. *Oncogene* 31, 4630-4638.

Zheng, Z. Y., Tian, L., Bu, W., Fan, C., Gao, X., Wang, H., Liao, Y. H., Li, Y., Lewis, M. T., Edwards, D., *et al.* (2015). Wild-type N-Ras, overexpressed in basal-like breast cancer, promotes tumor formation by inducing IL-8 secretion via JAK2 activation. *Cell reports* 12, 511-524.

Zill, O. A., Banks, K. C., Fairclough, S. R., Mortimer, S. A., Vowles, J. V., Mokhtari, R., Gandara, D. R., Mack, P. C., Odegaard, J. I., Nagy, R. J., *et al.* (2018). The Landscape of Actionable Genomic Alterations in Cell-Free Circulating Tumor DNA from 21,807 Advanced Cancer Patients. *Clin Cancer Res* 24, 3528-3538.

Zubairy, S., and Oesterreich, S. (2005). Estrogen-repressed genes -- key mediators of estrogen action? *Breast Cancer Res* 7, 163-164.

KEY RESOURCES TABLE

REAGENT or RESOURCE	SOURCE	IDENTIFIER
Antibodies		
Mouse monoclonal NF1 (against aa2471-2839, 1:200)	This study	
Rabbit polyclonal NF1 (against aa2471-2839)	This study	
NF1 (against aa2760-2839)	Bethyl Laboratories	Cat#A300-140A; RRID:AB_2149790
NF1 (against N-terminus, 1:500)	Cell Signaling Technology	Cat#14623; RRID:AB_2798543
ER- α (1:500)	Cell Signaling Technology	Cat#8644; RRID:AB_2617128
ER- α (HC-20)	Santa Cruz Biotechnology	Cat#sc-8002X; RRID:AB_627558
ER- α (F-10, ChIP grade, 1:5000 for Western blots)	Santa Cruz Biotechnology	Cat# sc-8002X; RRID:AB_627558
phospho-ER- α (Ser118, 1:500)	Millipore-Sigma	Cat#05-793; RRID:AB_310004
ERK1/2 (1:500)	Cell Signaling Technology	Cat#9102; RRID:AB_330744
Phospho-ERK1/2 (Thr202/Tyr204, 1:500)	Cell Signaling Technology	Cat#9101; RRID:AB_331646
AKT (1:500)	Cell Signaling Technology	Cat#4691; RRID:AB_915783
Phospho-AKT (Ser473, 1:500)	Cell Signaling Technology	Cat#4060; RRID:AB_2315049
His-tag (1:1000)	Cell Signaling Technology	Cat#2365; RRID:AB_2115720
Ran (1:1000)	Cell Signaling Technology	Cat#4462; RRID:AB_2284873
Histone-3 (1:1000)	Cell Signaling Technology	Cat#4499; RRID:AB_10544537
DNA-PKcs (1:1000)	Cell Signaling Technology	Cat#4602; RRID:AB_10692482
K48-linkage specific polyubiquitin (1:1000)	Cell Signaling Technology	Cat#8081; RRID:AB_10859893
α/β -tubulin (1:2000)	Cell Signaling Technology	Cat#2148; RRID:AB_2288042
α -tubulin (1:10,000)	Santa Cruz Biotechnology	Cat#sc-5286; RRID:AB_628411
p120/RasGAP (1:1000)	Santa Cruz Biotechnology	Cat#sc-63; RRID:AB_628206
SRC-1 (1:1,000)	Santa Cruz Biotechnology	Cat#sc-6096; RRID:AB_661355
HDAC1 (1:1,000)	Santa Cruz Biotechnology	Cat#sc-81598; RRID:AB_2118083
GAPDH (1:10,000)	Santa Cruz Biotechnology	Cat#sc-32233; RRID:AB_627679
Normal Mouse IgG	Santa Cruz Biotechnology	Cat# sc-2025; RRID:AB_628411
Normal Rabbit IgG	Millipore-Sigma	Cat# 12-370; RRID:AB_145841
Bacterial and Virus Strains		
BL21 (DE3)	Agilent	Cat#200131

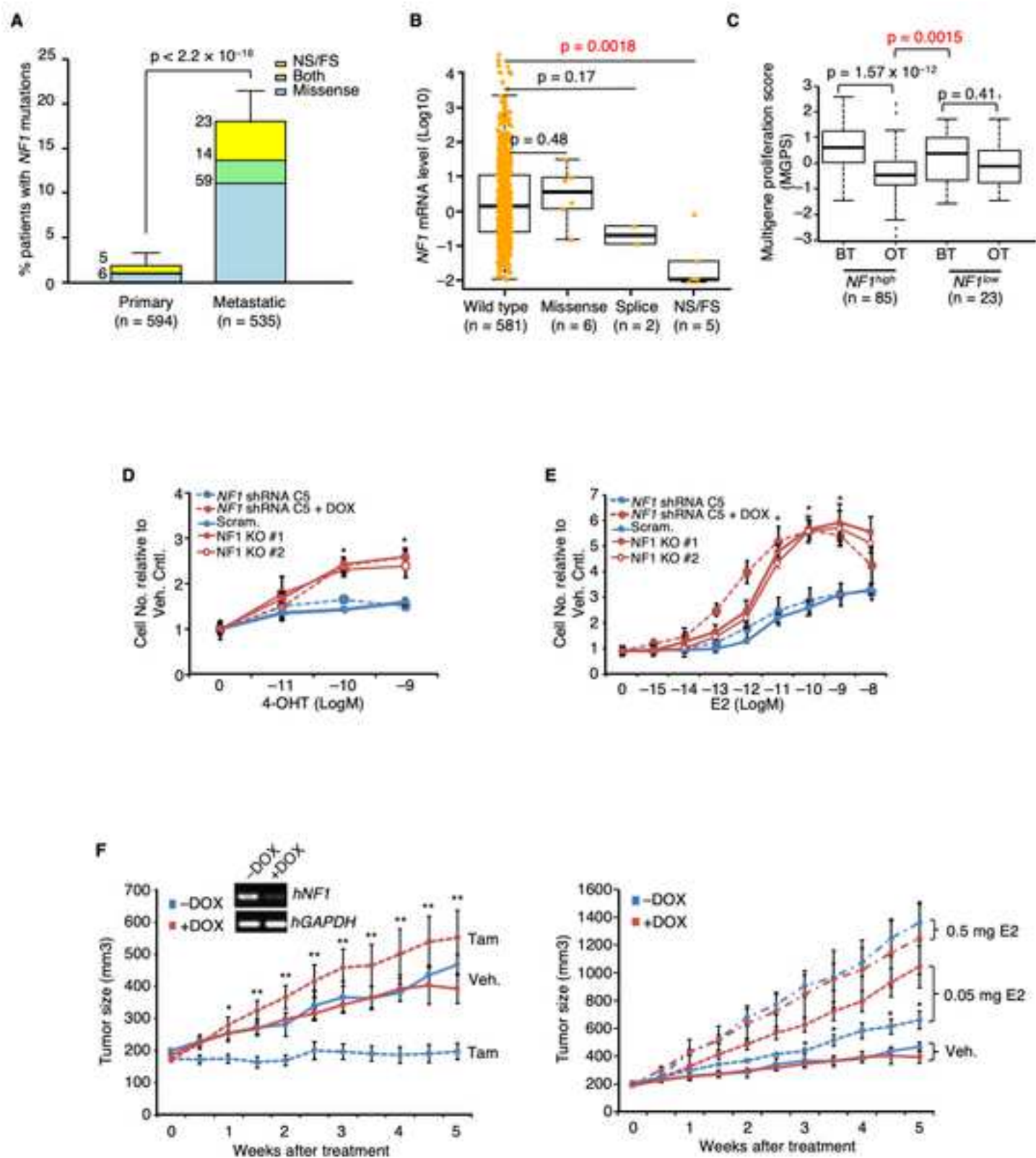
Biological Samples		
Patient-derived xenografts (PDX) WHIM16	(Li et al., 2013)	N/A
Chemicals, Peptides, and Recombinant Proteins		
17 β -estradiol (E2)	Sigma-Aldrich	Cat#E8875
Cyclodextran-encapsulated “water-soluble” E2	Sigma-Aldrich	Cat#E4389
(Z)-4-hydroxytamoxifen (4-OHT)	Sigma-Aldrich	Cat#H7904
Doxycycline (DOX)	Sigma-Aldrich	Cat#D9891
Human epidermal growth factor (EGF)	Sigma-Aldrich	Cat#E4127
Leptomycin B (LMB)	Sigma-Aldrich	Cat#L2913
Bufalin	Sigma-Aldrich	Cat#B0261
Phenylmethanesulfonyl fluoride (PMSF)	Sigma-Aldrich	Cat#78830
DMSO	Sigma-Aldrich	Cat#D8418
Ethanol	Sigma-Aldrich	Cat#E7023
MG132	Millipore-Sigma	Cat#474790
Polybrene	Millipore-Sigma	Cat#TR-1003-G
Trametinib	Selleck Chemicals, MedChem Express, or Novartis	Cat#S2673 or Cat#HY-10999A
Dabrafenib	Selleck Chemicals or MedChem Express	Cat#S2807 or Cat#HY-14660A
Fulvestrant	MedChem Express	Cat#HY-13636
Binimetinib	MedChem Express	Cat#HY-15202
Selumetinib	Selleck Chemicals or MedChem Express	Cat#S1008 or Cat#HY-50706
Recombinant ER α protein	ThermoFisher Scientific	Cat#A15674
Critical Commercial Assays		
TruSeq RNA Library Prep Kit	Illumina	Cat# RS-122-2001
KAPA Library Quantification Kit	Kapa Biosystems	Cat# KR0405
Deposited Data		
RNA-Seq	GEO	GSE142479
Experimental Models: Cell Lines		
MCF-7	ATCC	Cat#HTB-22; RRID:CVCL_0031
ZR-75B	A gift from Marc E. Lippman (Georgetown Univ., Med. Cntr.)	RRID:CVCL_5614
T47D	ATCC	Cat#HTB-133; RRID:CVCL_0553
Experimental Models: Organisms/Strains		
Athymic nude mice	Envigo	N/A
SCID/bg	Envigo	N/A
Oligonucleotides (5' \rightarrow 3')		
Scrambled shRNA (<u>antisense sequences</u>)	Dharmacon	CTTACTCTCGCCCAAGC GAGAG
NF1-C5 shRNA (<u>antisense sequences</u>)	Dharmacon	TTGGTCCGTATTTGAAG TC
NF1-C6 shRNA (<u>antisense sequences</u>)	Dharmacon	TAAGTAATGCGATATTG AG
NF1-I417M gRNA for CRISPR knock-in	This study	AATACCTTTTGGACTTA CAT

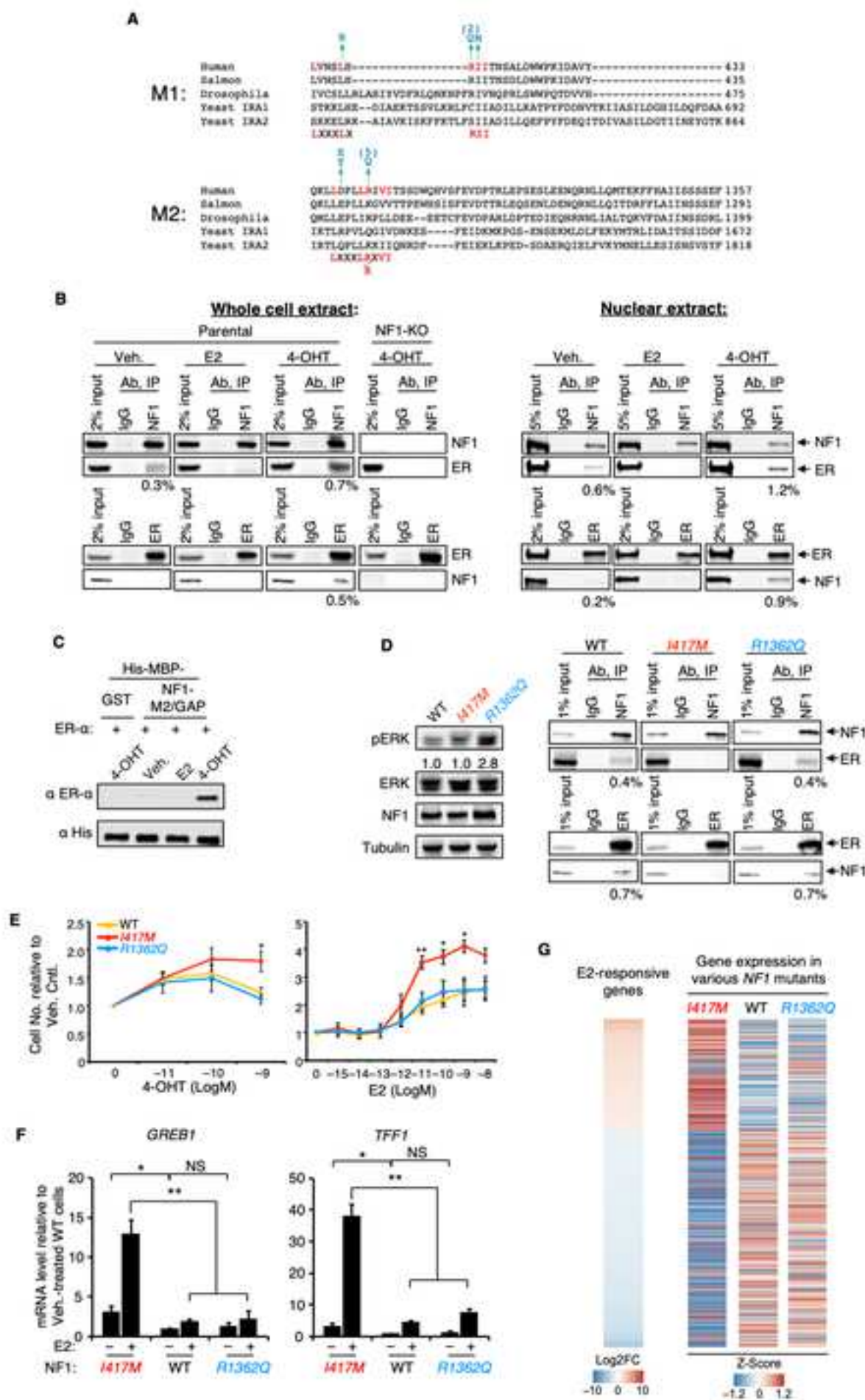
NF1-I417M ssODN for CRISPR knock-in	This study	CAGAATTCACCTTCTAC ATTTCACTATGTGCTGG TAAATTCCTCCATCGG ATGATCACAAACGTAA GTCCAAAAGGTATTGCT AAATTACTAAAAAATT TTTTCTTTCTTTTCTTT GCG
NF1-R1362Q gRNA for CRISPR knock-in	This study	GGCACACACTTCGAAGT TGA
NF1-R1362Q ssODN for CRISPR knock-in	This study	GACTGAAAAGTTCTTCC ATGCCATCATCAGTTCC TCCTCAGAATCCCACC TCAGCTGCAAAGTGTGT GCCACTGTTTATACCAG GTATGCTTACAGTTAGA GATTACCATTATTAATC TAAAG
Scrambled for CRISPR knock-out	This study	GCACTACCAGAGCTAA CTCA
NF1-KO#1 for CRISPR knock-out	GenScript	TCTTTAGTCGCATTTCT ACC
NF1-KO#2 for CRISPR knock-out	GenScript	AACTGGAAAAATGTCT TGC
Forward primer for cloning NF1-R1362Q	This study	CCCCCCCCAGCTGCAAA GCGTGTGCCAC
Reverse primer for cloning NF1-R1362Q	This study	GTGGCACACGCTTTGCA GCTGGGGGGGGG
Forward primer for cloning NF1-K1444R	This study	GGCCTGAAGCTGATGA GCAGGATTCTGCAGAG CATTGCC
Reverse primer for cloning NF1-K1444R	This study	GGCAATGCTCTGCAGA ATCCTGCTCATCAGCTT CAGGCC
Forward primer for cloning NF1-R2258*	This study	GCTGCATCTCCAAGTGA GTGAGCCACGGC
Reverse primer for cloning NF1-R2258*	This study	GCCGTGGCTCACTCACT TGGAGATGCAGC
Forward primer for cloning NF1-Y2285*	This study	GGCCCCGACACCTAAA ACTCCCAGGTGC
Reverse primer for cloning NF1-Y2285*	This study	GCACCTGGGAGTTTTAG GTGTCGGGGGCC
Forward primer for cloning NF1-R2450*	This study	GTGAGCGAGGAAGTGT GAAGCCGGTGCAGCCT G
Reverse primer for cloning NF1-R2450*	This study	CAGGCTGCACCGGCTTC ACACTTCCTCGCTCAC
Forward primer for cloning NF1-I417M	This study	TCCCTGCACCGGATGAT ACCAACAGCG
Reverse primer for cloning NF1-I417M	This study	CGCTGTTGGTGTATCATC CGGTGCAGGGA
Forward primer for cloning NF1-I417A/I418A	This study	TGAACTCCCTGCACCGG GCCGCCACCAACAGCG CCCTGG

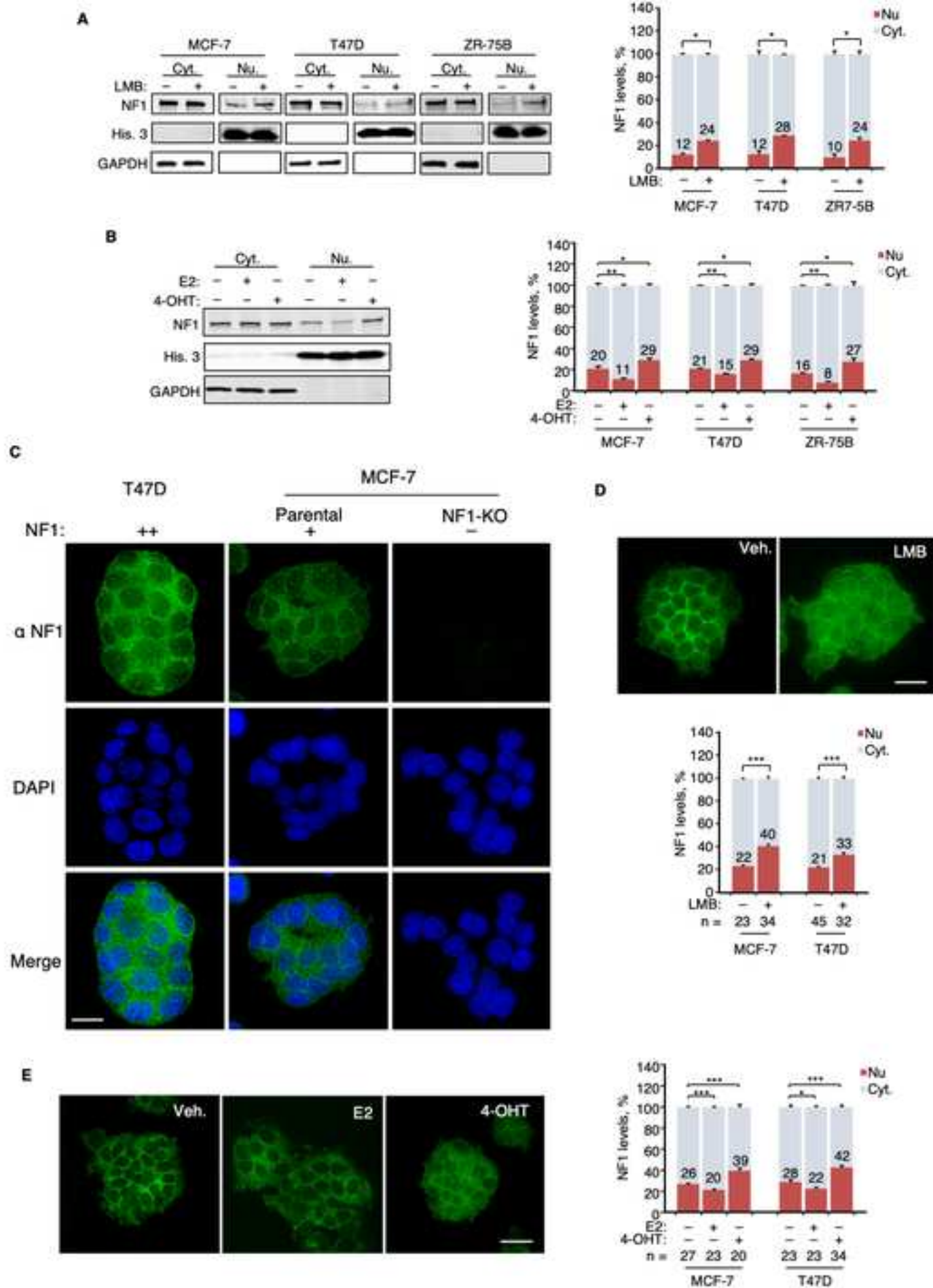
Reverse primer for cloning NF1-I417A/I418A	This study	CCAGGGCGCTGTTGGTG GCGGCCCGGTGCAGGG AGTTCA
Forward primer for cloning NF1-V1308A/I1309A	This study	CCCTGCTGAGGATCGCG GCCACCAGCAGCGACT G
Reverse primer for cloning NF1-V1308A/I1309A	This study	CAGTCGCTGCTGGTGGC CGCGATCCTCAGCAGG G
qPCR primer GREB1-F	(Zheng et al., 2005)	CCCCGTGGCCCCGCAGA G
qPCR primer GREB1-R	(Zheng et al., 2005)	AGGATGAGCCCCGAGGA GGAGGACA
qPCR primer TFF1-F	(Zheng et al., 2005)	ATGGCCACCATGGAGA ACAAGG
qPCR primer TFF1-R	(Zheng et al., 2005)	CTAAAATTCACACTCCT CTTCTGG
qPCR primer PRG-F	(de Cremoux et al., 2004)	CGCGCTCTACCCTGCAC TC
qPCR primer PRG-R	(de Cremoux et al., 2004)	TGAATCCGGCCTCAGGT AGTT
qPCR primer NRIP-F	(Berto et al., 2018)	ATGCAGCAAAGCGGAA GAG
qPCR primer NRIP-R	(Berto et al., 2018)	CCTTTAGGCACACTGTC AACC
qPCR primer RET-F	(Borromeo et al., 2016)	AAAGTGGCATTGGGCCT CTAC
qPCR primer RET-R	(Borromeo et al., 2016)	GCAGGGCATGGACGTA CAG
qPCR primer MYB-F	(Wang et al., 2018)	GAAAGCGTCACTTGGG GAAAA
qPCR primer MYB-R	(Wang et al., 2018)	TGTTTCGATTTCGGGAGAT AATTGG
qPCR primer MYC-F	(Ding et al., 2019)	TCCCTCCACTCGGAAGG AC
qPCR primer MYC-R	(Ding et al., 2019)	CTGGTGCATTTTCGGTT GTTG
qPCR primer hGAPDH-F	(Zheng et al., 2005)	ACCCACTCCTCCACCTT TG
qPCR primer hGAPDH-R	(Zheng et al., 2005)	CTCTTGTGCTCTTGCTG GG
qPCR primer hNF1-F	(Paschou and Doxakis, 2012)	GCTTTCGTATAAGCCCT CACAA
qPCR primer hNF1-R	(Paschou and Doxakis, 2012)	GCGGAATTGGTGATGAT TCGAT
qPCR primer NF1-NCI-F	This study	ATCAACCCTGCCATCGT GAG
qPCR primer NF1-NCI-R	This study	GGTAAACAGCACGTGG TTGG
ChIP-qPCR primer GREB1 ERE (site #1)-F	(Gates et al., 2018)	CAGGGGCTGACAACCTG AAAT
ChIP-qPCR primer GREB1 ERE (site #1)-R	(Gates et al., 2018)	GAGAGGGTGGTGACAC TTGG
ChIP-qPCR primer GREB1 ERE (site #2)-F	(Lin et al., 2004)	AGCAGTGAAAAAAGT GTGGCAACTGGG

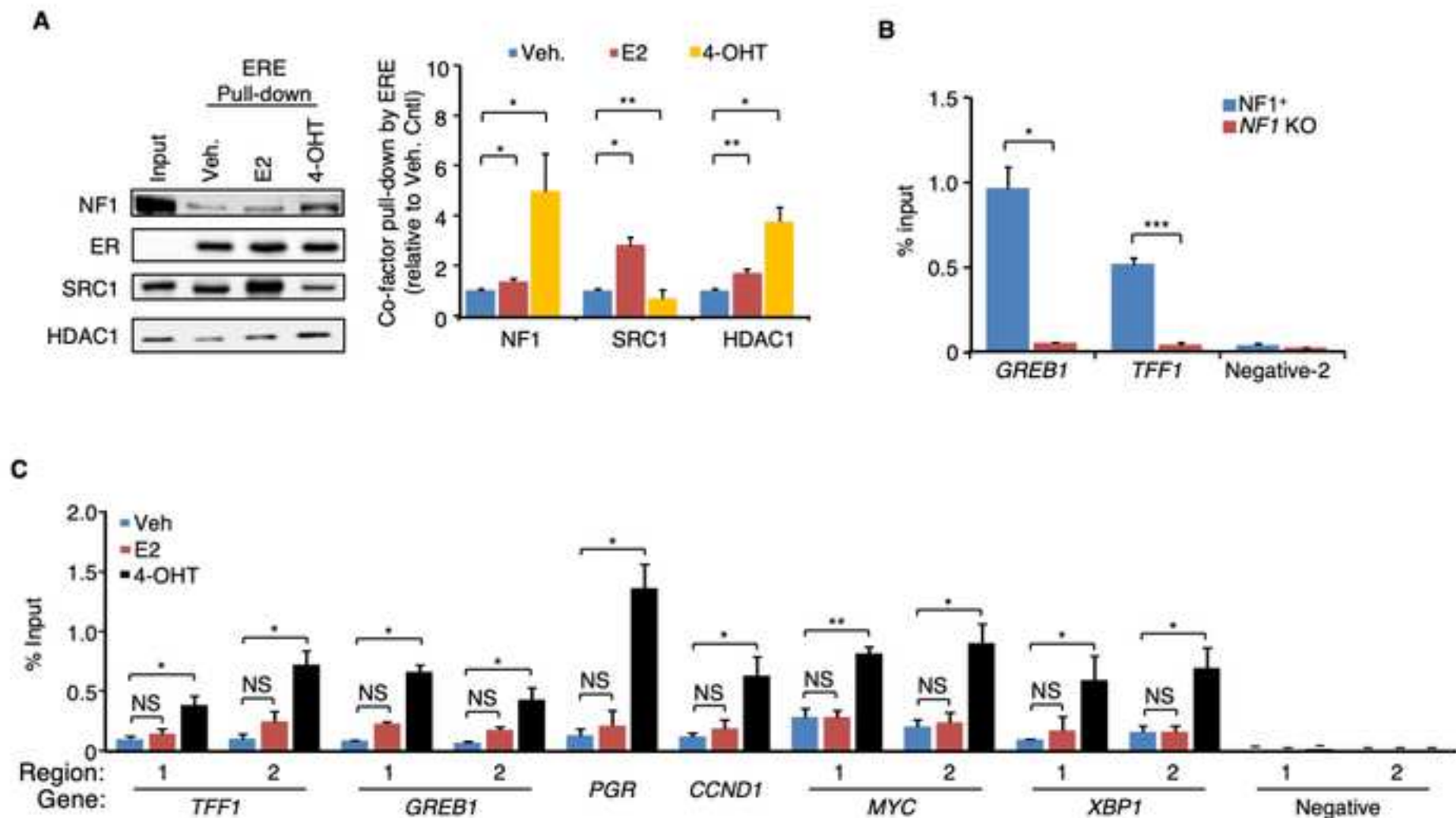
ChIP-qPCR primer GREB1 ERE (site #2)-R	(Lin et al., 2004)	GACCCACAGAAATGAA AAGGCAGCAAACCT
ChIP-qPCR primer TFF1 ERE (site #1)-F	(Kininis et al., 2009)	CCTGGATTAAGGTCAGG TTGGA
ChIP-qPCR primer TFF1 ERE (site #1)-R	(Kininis et al., 2009)	TCTTGGCTGAGGGATCT GAGA
ChIP-qPCR primer TFF1 ERE (site #2)-F	(Won Jeong et al., 2012)	GTCGTTGCCAGCGTTTC
ChIP-qPCR primer TFF1 ERE (site #2)-R	(Won Jeong et al., 2012)	CTTCTCCACGCCCTGTA AATTT
ChIP-qPCR primer PGR ERE-F	This study, designed based on (Carroll et al., 2006)	GTAATCAAATCTGTGGC ACACC
ChIP-qPCR primer PGR ERE-R	This study, designed based on (Carroll et al., 2006)	GTCCTCAAAAACCTCAAT TTCATAAGT
ChIP-qPCR primer CCND1 ERE-F	(Karmakar et al., 2013)	CAGTTTGTCTTCCCGGG TTA
ChIP-qPCR primer CCND1 ERE-R	(Karmakar et al., 2013)	TCATCCAGAGCAAACA GCAG
ChIP-qPCR primer MYC ERE (site #1)-F	(Glont et al., 2019)	GCTCTGGGCACACACAT TGG
ChIP-qPCR primer MYC ERE (site #1)-R	(Glont et al., 2019)	GGCTCACCCCTTGCTGAT GCT
ChIP-qPCR primer MYC ERE (site #2)-F	(Harrod et al., 2017)	AGGGTGAGGTCAAGCA TTTG
ChIP-qPCR primer MYC ERE (site #2)-R	(Harrod et al., 2017)	TGGCCTTGAACCCATAC TTC
ChIP-qPCR primer XBP1 ERE (site #1)-F	(Glont et al., 2019)	ATACTTGGCAGCCTGTG ACC
ChIP-qPCR primer XBP1 ERE (site #1)-R	(Glont et al., 2019)	GGTCCACAAAGCAGGA AAAA
ChIP-qPCR primer XBP1 ERE (site #2)-F	(Carroll et al., 2005)	TTGCTGTGCAAACAATA GCC
ChIP-qPCR primer XBP1 ERE (site #2)-R	(Carroll et al., 2005)	GTCCAAGGGCACATTCT CAT
ChIP-qPCR primer ERE-negative region-1-F	(Carroll et al., 2005)	AATACCTGAGGACCCC AACC
ChIP-qPCR primer ERE-negative region-1-R	(Carroll et al., 2005)	TCTTCACTCTCCTCGCA TTG
ChIP-qPCR primer ERE-negative region-2-F	(Carroll et al., 2006)	GAGGCTGTGCTTGGAGT AGG
ChIP-qPCR primer ERE-negative region-2-R	(Carroll et al., 2006)	CGTTTCCCCTGTGAAAG GTA
Recombinant DNA		
pMD2.G	Addgene	Cat#12259
pSPAX2	Addgene	Cat#12260
pINDUCER11-scrambled shRNA	This study	
pINDUCER11-NF1 shRNA clone 5	This study	
pINDUCER11-NF1 shRNA clone 6	This study	
pLentiCRISPR v2-scramble	This study	
pLentiCRISPR v2-NF1 clone 1	GenScript	N/A
pLentiCRISPR v2-NF1 clone 2	GenScript	N/A
pDONR225-NF1	A gift from the RAS Initiative at the Frederick National Laboratory for Cancer Research at NCI	N/A

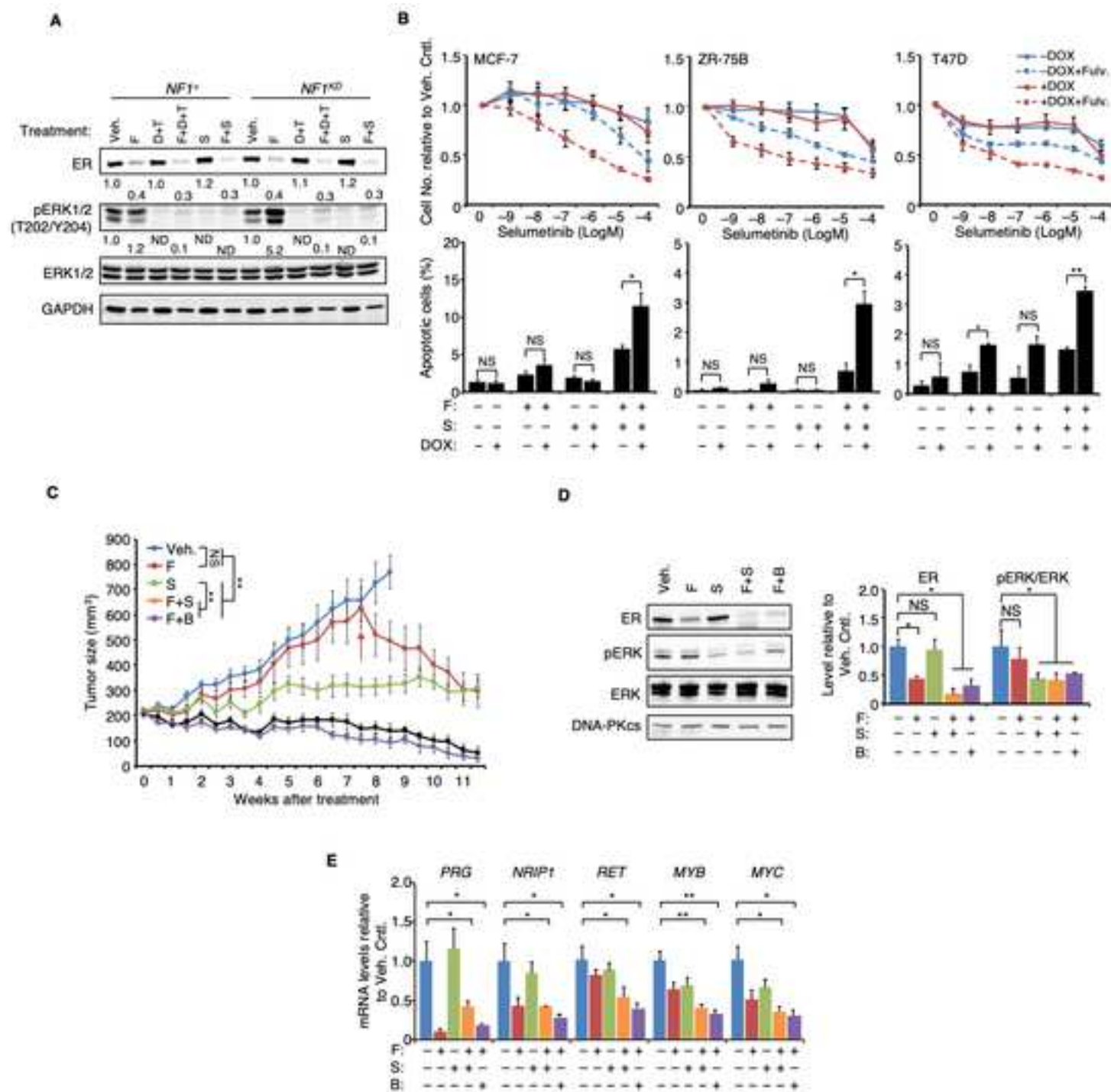
pCL-FLAG	(Zheng et al., 2012)	N/A
pCL-FLAG-NF1	This study	
pCL-FLAG-NF1-R2258*	This study	
pCL-FLAG-NF1-Y2285*	This study	
pCL-FLAG-NF1-R2450*	This study	
pCL-FLAG-NF1-R1362Q	This study	
pCL-FLAG-NF1-K1444R	This study	
pCL-FLAG-NF1-I417M	This study	
pCL-FLAG-NF1-V1308A/I1309A	This study	
pM-NF1	This study	
pM-NF1-R1362Q	This study	
pM-NF1-K1444R	This study	
pM-NF1-I417M	This study	
pM-NF1-I417A/I418A	This study	
pM-NF1-V1308A/I1309A	This study	
pDEST566-GST	This study	
pDEST566-NF1-M2/GAP	A gift from the RAS Initiative at the Frederick National Laboratory for Cancer Research at NCI	N/A
SpCas9(BB)-2A-GFP(PX458)	Addgene	Cat# 48138; RRID: Addgene_48138
pGL4.70-RLuc	Promega	Cat#E688A
pGL2-ERE-Luc	A gift from Donald P. McDonnell (Duke Univ.)	(Hall and McDonnell, 1999)
5×Gal4-Luc	Promega	Cat#E2440
pVP16-ERα	A gift from Donald P. McDonnell	(Chang et al., 1999)
pVP16-SRC1	A gift from Donald P. McDonnell	(Chang et al., 1999)
pVP16-NCOR1	A gift from Donald P. McDonnell	(Chang et al., 1999)
Software and Algorithms		
ImageJ	(Schneider et al., 2012)	https://imagej.nih.gov/ij/
SoftWorx v7.0	GE Healthcare	N/A
FlowJo	FlowJo	N/A
Bowtie2	(Langmead and Salzberg, 2012)	http://bowtie-bio.sourceforge.net/bowtie2/index.shtml
RSEM v1.2.31	(Li and Dewey, 2011)	https://deweylab.github.io/RSEM/
R 3.3.4	R Core Team	N/A











Supplemental data inventory

Supplemental figures to the main figures are submitted separately. This paper also has the following supplemental tables that are submitted as supplemental spreadsheets:

Table S1. Supplemental to main Figure 1. Non-silent *NFI* mutations identified by sequencing circulating tumor DNA in a metastatic ER⁺ breast cancer cohort.

Table S2. Supplemental to main Figure 1. Multi Gene Proliferation Scores (MGPS) of samples in the Z1031 trial.

Table S3. Supplemental to main Figure 2. E2 and 4-OHT modulated gene expression changes in the MCF-7 cell model.

Table S4. Supplemental to main Figure 2. Hallmark Pathway enrichment validation in patient data in TCGA and METABRIC.

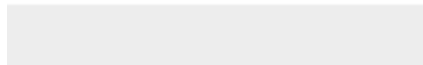
Table S5. Supplemental to main Figure 3. Gene expression as analyzed by RNA-seq in MCF-7 cells carrying wild-type *NFI* or an *NFI* Knock-in mutation.

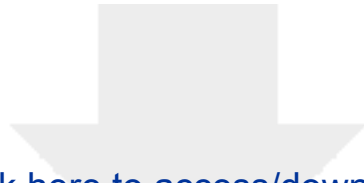


[Click here to access/download](#)

Supplemental Videos and Spreadsheets

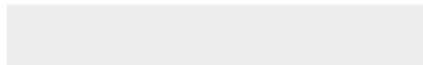
Table S1 NF1 mutations in metastatic BC R2.xlsx





[Click here to access/download](#)

Supplemental Videos and Spreadsheets
Table S2 MGPS analysis in the AI trial R2.xlsx

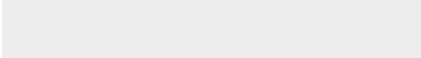


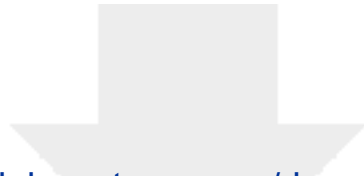


[Click here to access/download](#)

Supplemental Videos and Spreadsheets

Table S3 Diff gene expression by RNAseq in MCF7
R2.xlsx





[Click here to access/download](#)

Supplemental Videos and Spreadsheets

Table S4. RNAseq validation in TCGA_Metabric R2.xlsx





[Click here to access/download](#)

Supplemental Videos and Spreadsheets
Table S6 RNAseq in KI cells R2.xlsx





[Click here to access/download](#)

Supplemental Videos and Spreadsheets
Table S5 RNAseq in KI cells R3.xlsx

